Acyl-coenzyme a binding protein (ACBP) - a risk factor for cancer diagnosis and an inhibitor of immunosurveillance

Léa Montégut, Peng Liu, Liwei Zhao, María Pérez-Lanzón, Hui Chen, Misha Mao, Shuai Zhang, Lisa Derosa, Julie Le Naour, Flavia Lambertucci, et al.

Montégut *et al. Molecular Cancer* (2024) 23:187
https://doi.org/10.1186/s12943-024-02098-5

Molecular Cancer

RESEARCH Open Access

Acyl-coenzyme a binding protein (ACBP) - a risk factor for cancer diagnosis and an inhibitor of immunosurveillance

Léa Montégut[1,2,3], Peng Liu[1,2], Liwei Zhao[1,2], María Pérez-Lanzón[1,2], Hui Chen[1,2,3], Misha Mao[1,2], Shuai Zhang[1,2,4], Lisa Derosa[3,5], Julie Le Naour[1,2,3], Flavia Lambertucci[1,2], Silvia Mingoia[1,6], Uxía Nogueira-Recalde[1,2,7], Rafael Mena-Osuna[8], Irene Herranz-Montoya[9], Nabil Djouder[9], Sylvain Baulande[10], Hui Pan[1,2,3], Adrien Joseph[1,11], Meriem Messaoudene[12], Bertrand Routy[12,13], Marine Fidelle[5,14], Tarek Ben Ahmed[15,16], Olivier Caron[15,16], Pierre Busson[17], David Boulate[18,19,20], Mélanie Deschasaux-Tanguy[21,22], Nathalie Arnault[21,22], Jonathan G. Pol[1,2], Eliane Piaggio[8], Mathilde Touvier[21,22], Laurence Zitvogel[2,3,5,23], Suzette Delaloge[5,16], Isabelle Martins[1,2*] and Guido Kroemer[1,2,24*]

Abstract

Background The plasma concentrations of acyl coenzyme A binding protein (ACBP, also known as diazepam-binding inhibitor, DBI, or 'endozepine') increase with age and obesity, two parameters that are also amongst the most important risk factors for cancer.

Methods We measured ACBP/DBI in the plasma from cancer-free individuals, high-risk patients like the carriers of *TP53* or *BRCA1/2* mutations, and non-syndromic healthy subjects who later developed cancer. In mice, the neutralization of ACBP/DBI was used in models of non-small cell lung cancer (NSCLC) and breast cancer development and as a combination treatment with chemoimmunotherapy (chemotherapy + PD-1 blockade) in the context of NSCLC and sarcomas. The anticancer T cell response upon ACBP/DBI neutralization was characterized by flow cytometry and single-cell RNA sequencing.

Results Circulating levels of ACBP/DBI were higher in patients with genetic cancer predisposition (*BRCA1/2* or *TP53* germline mutations) than in matched controls. In non-syndromic cases, high ACBP/DBI levels were predictive of future cancer development, and especially elevated in patients who later developed lung cancer. In preclinical models, ACBP/DBI neutralization slowed down breast cancer and NSCLC development and enhanced the efficacy of chemoimmunotherapy in NSCLC and sarcoma models. When combined with chemoimmunotherapy, the neutralizing monoclonal antibody against ACBP/DBI reduced the frequency of regulatory T cells in the tumor bed, modulated the immune checkpoint profile, and increased activation markers.

*Correspondence:
Isabelle Martins
isabelle.martins@inserm.fr
Guido Kroemer
kroemer@orange.fr

Full list of author information is available at the end of the article

Conclusion These findings suggest that ACBP/DBI acts as an endogenous immune suppressor. We conclude that elevation of ACBP/DBI constitutes a risk factor for the development of cancer and that ACBP/DBI is an actionable target for improving cancer immunosurveillance.

Keywords Precocious detection, Neuroendocrine factors, Non-small cell lung cancer, Immunosurveillance, Immunotherapy

Background

Acyl-coenzyme A binding protein (ACBP), which is encoded by *diazepam binding inhibitor* (*DBI*), is a phylogenetically ancient, small (~10 kDa) protein. ACBP/DBI can be found intracellularly as a protein interacting with activated medium to long-chain fatty acids and other lipids, facilitating their transport and utilization in anabolic processes (including the synthesis of ceramides, glycerolipids, phospholipids and steroids) or in mitochondrial fatty acid oxidation [1]. Extracellularly, ACBP/DBI acts as a soluble factor that binds to the same receptor as does diazepam, a prototypic benzodiazepine [2, 3]. ACBP/DBI indeed competitively displaces diazepam from its binding site in the pentameric gamma-aminobutyric acid (GABA) receptor type A. For this reason, ACBP/DBI and its fragments are also called 'endozepines' [4, 5]. Thus, ACBP/DBI acts like a neuroendocrine agent that, embedded in multiple regulatory pathways and intertwined with other factors, contributes to the regulation of appetite and body composition [3].

Plasma ACBP/DBI levels increase with adiposity, meaning that they strongly correlate with the body mass index (BMI) in healthy persons [6–8]. In addition, ACBP/DBI levels in the plasma increase in the context of chronological aging, independently from the correlation with BMI [3, 8]. We have observed two types of derangement in these correlations between ACBP/DBI plasma concentrations and age or BMI. In healthy individuals that were diagnosed with cardiovascular disease within 9 years after drawing blood for ACBP/DBI quantification, the levels of ACBP/DBI were disproportionally high, and this effect was independent from BMI and age. This observation suggested that ACBP/DBI might correlate with the biological (rather than only chronological) aging process that is associated with the development of cardiovascular disease [9]. Moreover, in patients that had been diagnosed with cancer, the correlation between ACBP/DBI levels and age or BMI was lost, suggesting the disruption of homeostatic circuitries [8]. In patients, the development of metabolic syndrome is commonly evaluated by clinical criteria such as elevated blood pressure, hypertriglyceridemia, low high-density lipoprotein cholesterol, high waist circumference and hyperglycemia. Of note, the presence of all or a subset of these metabolic criteria was associated with increased risk of non-small cell lung cancer (NSCLC) development in a prospective general-population study, pleading in favor of a more thorough metabolic assessment of lung cancer patients [10].

In preclinical experiments, inhibition of ACBP/DBI has positive effects on a variety of (patho)physiological parameters. Its genetic inhibition in model organisms prolongs lifespan [11–13]. Its knockout or neutralization by antibodies (which act on the extracellular pool of ACBP/DBI) protect various organs against cell loss and inflammation induced by ischemia, toxic agents and dietary insult [14, 15]. ACBP/DBI is overexpressed in a wide variety of cancer types [1], and most studies have focused on the intracellular contribution of ACBP/DBI to cancer cell metabolism. Thus, it has been demonstrated in the context of NSCLC [16] and glioblastoma [17, 18] that ACBP sustains cellular bioenergetics by stimulating fatty acid oxidation. However, the effects of systemic ACBP/DBI inhibition on cancer has not been investigated.

Here, we investigated whether plasma ACBP/DBI levels might be elevated in individuals at high risk of developing a cancer in the forthcoming years and found that ACBP/DBI was indeed overabundant in the plasma of persons at risk. We observed that antibody-mediated neutralization of extracellular ACBP/DBI protects against NSCLC and synergizes with chemoimmunotherapy against NSCLC and sarcoma. This latter effect correlated with changes in the composition of the T cells infiltrating tumors that suggest reduced local immunosuppression and improved immune activation. These findings plead in favor of a cancer-relevant immunomodulatory effect of ACBP/DBI.

Methods

Patients

Li-Fraumeni syndrome patients

The LIFSCREEN clinical trial (NCT01464086) was originally designed to measure the benefits of whole-body MRI screening to detect early-stage cancer cases in patients carrying germline TP53 mutations (*gTP53m*) [19, 20]. The primary outcome was to assess whether the inclusion of whole-body MRI in the evaluation of patients would influence their overall survival. The secondary aim of the study was to create a collection of serum and plasma samples to establish a library for future investigations into new tumor biomarkers. In total, 107 individuals, consisting of 78 women and 29 men from 75 distinct families, were recruited for the study. The present cohort

includes the $N=38$ patients bearing *gTP53m* who provided a signed agreement for the LIFSCREEN translational study part and for whom a sufficient volume of frozen plasma at inclusion was available. This sub-study was approved as part of a screening for inflammatory biomarkers by the steering committee of LIFSCREEN. For comparison, Li-Fraumeni syndrome (LFS) patients were matched by sex, BMI and age with cancer-free healthy patients from the previously published and publicly available DESIR cohort [9] to a 2:1 controls: cases ratio with the MatchIt R package. The resulting cohort has comparable values for sex, BMI and age between controls and LFS patients (Table S1).

Germline BRCA1/2 mutation carriers

Whole blood samples were collected at Gustave Roussy between 2013 and 2016, during a screening for *BRCA1* and *BRCA2* germline mutations among healthy individuals with a family history of breast or ovarian cancer. All samples were taken under similar material and psychological conditions: on the same premises, between around 10am and 12am, with the aim of screening, meaning that all patients were exposed to the same stress-inducing uncertainty. During the consultation, patients were asked to sign an informed consent form authorizing the use of the leftovers of the material collected for research purposes in addition to diagnostic. For each patient, 20 mL of peripheral blood was collected in EDTA tubes and kept at room temperature for less than 2 h until the plasma was separated. For this, the blood tubes were centrifuged for 15 min at 1700 g at 20 °C, plasma was homogenized, aliquoted and stored at -80 °C until use. Figure 1F represents the flowchart of the cohort. Table S2 summarizes the main patient characteristics.

Healthy volunteers

The healthy volunteers' cohort was constituted of baseline samples from the randomized, double-blinded, placebo-controlled interventional study on the prevention of cancer and cardiovascular disease by supplementation of antioxidant vitamins and minerals ("SUpplémentation en Vitamines et Minéraux AntioXydants", SU-VI-MAX, NCT00272428). A total of 13,017 patients were enrolled over a period of 8 years (1994–2002) and followed until 2007 [21, 22]. All patients signed informed consent forms to participate in the study, and this sub-study was approved by the steering committee of SUVIMAX. During the initial phase of the study, information regarding sociodemographic characteristics, smoking habits, medication usage, and overall health status was gathered through self-administered questionnaires. Additionally, trained nurses and physicians conducted a baseline clinical examination, which involved taking anthropometric measurements and obtaining blood samples from participants. The blood samples were collected in heparin tubes following a 12-hour fasting period. Among the 13,017 patients, we selected the $N=638$ patients that had never had malignancies at baseline but developed cancer during follow-up. They were matched with a 2:1 controls: cases ratio by sex, age, BMI, nutritional intervention group (placebo vs. vitamins and minerals), smoking status, season of blood draw and, for women, menopausal status (at baseline and at the date of cancer occurrence). The clinical characteristics of the cancer patients and their matched controls are summarized in Table S3.

Statistics

Statistical analysis of patients' datasets was performed on R (v. 4.2.0). The comparisons of ACBP/DBI concentrations between two groups were performed by unpaired, one-sided Student's t-test, following the hypothesis that cancer occurrence was associated with *increased* circulating levels of ACBP/DBI. Correlation analyses were performed with the *cor.test* function: Pearson's product moment correlation coefficients (r) were calculated, p-values were evaluated assuming that the r coefficients followed a t distribution and confidence intervals were computed based on Fisher's Z transform. Classification power was evaluated by computing receiver operating characteristic (ROC) curves and calculating the area under the curve (AUC) with the pROC package [23]. Wilcoxon rank sum tests were used for computing p-values of the AUC (different from 0.5). AUCs with their 95% confidence intervals were represented as forest plots. Survival data were plotted as Kaplan-Meier curves and analyzed by log-rank (Mantel-Cox) test.

ACBP/DBI quantification

Plasma concentrations of ACBP/DBI were measured in the same laboratory and by the same experimenter for all presented cohorts. Enzyme-linked immunosorbent assay (ELISA) was performed as previously described [7, 24]. Briefly, heparin plasma samples were diluted (1/20 for mouse, 1/50 for human) and incubated on capture antibody (MyBioSource, Cat# MBS768488, RRID: AB_3083599) coated plates for 2 h at 18–22 °C (room temperature, RT). They were detected by means of a biotin-conjugated antibody (LS Bio, Cat# LS-C299614, RRID:3083603), incubated 2 h at RT, and avidin-coupled horseradish peroxidase (avidin-HRP, BioLegend, Cat# 405103). The HRP substrate (Thermo Fisher Scientific, Cat# 34028) was incubated until sufficient color appeared, at which point 2 M sulfuric acid was added to quench the reaction. Absorbance was read at 450 nm on an automated plate reader within 15 min, and out-of-standard curve measurements were excluded. For germline *BRCA1/2* mutation carriers and their controls,

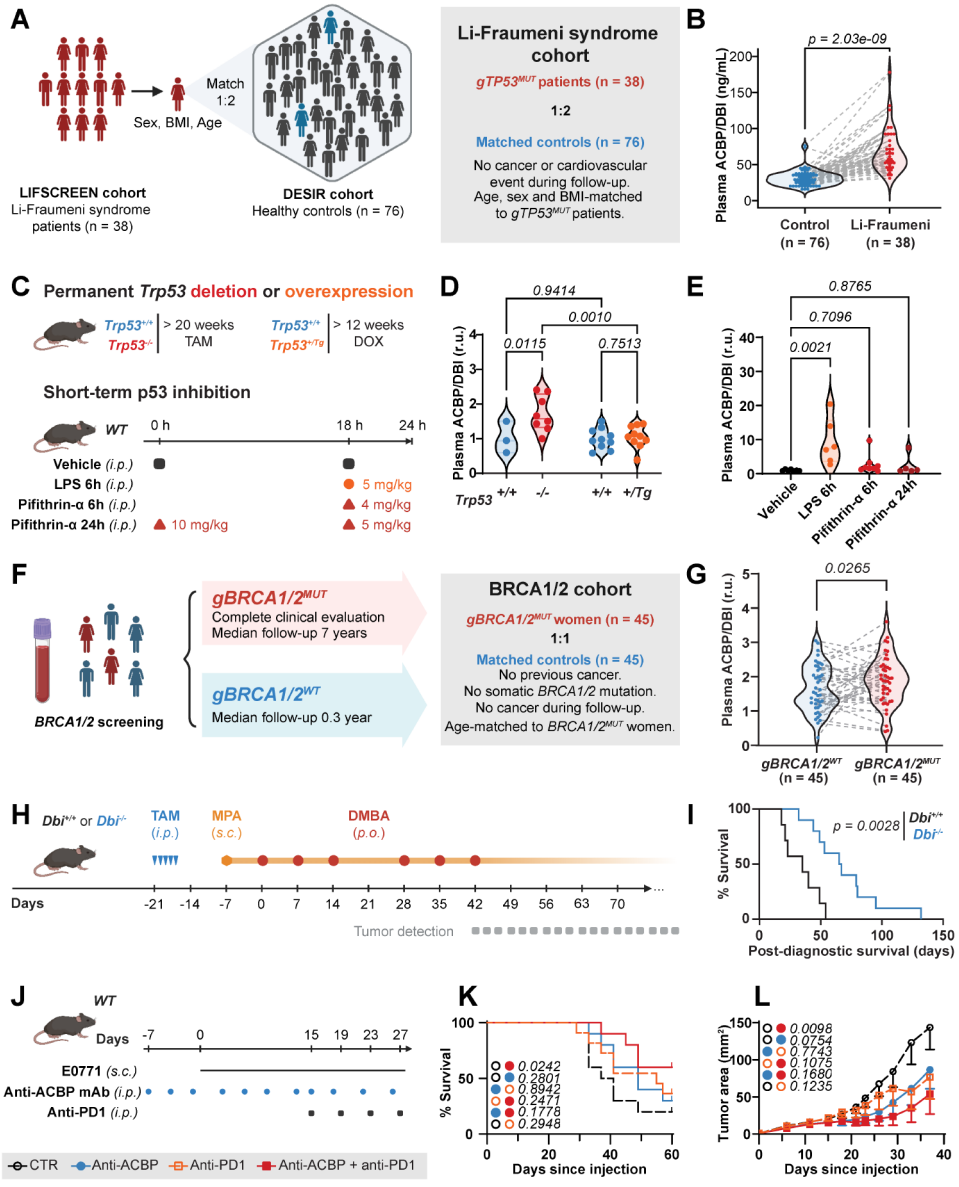

Fig. 1 ACBP/DBI is elevated in the plasma from patients with genetic predisposition to cancer. Plasma from patients with Li-Fraumeni syndrome (LFS) bearing *gTP53*^{MUT} were collected at inclusion in the LIFSCREEN trial for MRI-screening of new malignancies. Each patient with LFS was matched by sex, body mass index (BMI) and age with two healthy patients from the DESIR cohort (A), and plasma ACBP/DBI was measured by ELISA. LFS patients had increased ACBP/DBI levels compared to healthy volunteers (one-sided unpaired Student's *t*-test, B). TP53 modulation in mice was achieved in vivo either in the long-term by genetic manipulations (tamoxifen-induced knockout or constitutive overexpression of the *Trp53* gene) or at short-term by intraperitoneal injections of the TP inhibitor pifithrin-α (C), and plasma ACBP/DBI was measured by ELISA (D, E). Bacterial lipopolysaccharide (LPS) was used as positive control for short-term induction of ACBP/DBI in mice. Plasma specimens were collected from a cohort of women enrolled in a screening campaign for *BRCA1/2* mutations. *N* = 45 mutated: control pairs were randomly created by age-matching patients bearing germline *BRCA1/2* mutations with controls who were exempt of known previous or future cancer as well as of somatic *BRCA1/2* mutations (F). Patients with germline mutations in either *BRCA1* or *BRCA2* had significantly higher plasma levels of ACBP/DBI than their age-matched controls (one-sided paired Student's *t*-test, G). Breast cancer was induced by combination of a subcutaneous implant releasing medroxyprogesterone acetate (MPA) and weekly gavage with dimethylbenzanthracene (DMBA), after a 5-day tamoxifen induction period in *Ubc:Cre*$^{+/-}$*Acbp*$^{fl/fl}$ (i.e. *Acbp*$^{-/-}$, *n* = 9) or *Ubc:Cre*$^{-/-}$*Acbp*$^{fl/fl}$ (i.e. *Acbp*$^{+/+}$, *n* = 7) mice (H). Once diagnosed with breast cancer by palpation, *Acbp*$^{-/-}$ animals survived longer than their *Acbp*$^{+/+}$ littermates (I). Female C57Bl/6J mice were regularly treated intraperitoneally with an ACBP/DBI monoclonal antibody (or the corresponding isotype control, mouse IgG2a, both 5 mg/kg). E0771 cells (5.0×10^5 per mouse) were injected into the mammary fat pad, and mice were treated with four cycles of anti-PD1 monoclonal antibody (or the corresponding isotype control, rat IgG2a, 200 µg per cycle) (J). The combination of anti-ACBP/DBI with immune checkpoint blockade slowed down tumor growth (K) and prolonged survival (L). Survival curves were compared by log-rank (Mantel-Cox) test, while tumor growth speeds were assessed by linear mixed effect modeling on the https://kroemerlab.shinyapps.io/TumGrowth/ website

plasma was collected in EDTA tubes only relative quantifications were available for subsequent analyses.

Cell culture

C57Bl/6-derived cancer cell lines (TC1 cells expressing the luciferase enzyme, TC1-Luc, RRID: CVCL_4699, and MCA205, RRID: CVCL_VR90) were maintained in Dulbecco's Modified Eagle Medium (DMEM) supplemented with 10% fetal bovine serum (FBS) and 10 mM HEPES. MCA205 were transduced with lentiviral particles with the ZsGreen-OVA transgene that were produced in 293FT cells (Thermo Fisher, Cat# R70007) by co-transfecting the plasmid coding for the fluorescent protein ZsGreen coupled with ovalbumin (OVA) and puromycin resistance (pCDH_Zs-Green-OVA_puro, Fig. S5E), the lentiviral packaging plasmid psPAX2 (Addgene Cat# 12260), and the VSV-G envelope expressing plasmid (Addgene, Cat# 12259). After cytofluorometric sorting of $ZsGreen^+$ cells, single clones were put to grow under puromycin selection (5 µg/mL) to obtain stably transduced cells.

Mouse experiments

Animal housing and handling

C57Bl/6J mice were handled according to the Federation of European Laboratory Animal Science Associations (FELASA) guidelines, as approved by the local ethics committee (project numbers #24410, #31018, #49169, #50485 and #IACUC.015-2019). Animals were left untouched for at least one week of acclimatation, provided with food ad libitum and housed collectively in a temperature-controlled environment with 12-hour light-dark cycles.

Trp53 transgenic mice

Inducible knockout was induced in $Trp53^{lox/lox}$ mice [25], with either $UBC\text{-}cre/ERT2^{+/T}$ or $UBC\text{-}cre/ERT2^{-/-}$ [26] by feeding them with a tamoxifen diet (Envigo RMS, Cat. #TAM400/CreER) at 8 weeks of age for two weeks. Plasma from the resulting $Trp53^{+/+}$ and $Trp53^{-/-}$ littermates was collected in EDTA tubes at 30 weeks of age. Overexpression of *Trp53* was achieved by insertion of the *Tg.Trp53[MS-2] (+/T)* transgene [27] and plasmas were collected from p53-overexpressing mice and the corresponding controls between 20 and 25 weeks of age.

Induced breast cancer

Female *Ubc: Cre*, $Acbp^{fl/fl}$ mice under 8 weeks old were induced with five consecutive daily injections of tamoxifen (75 mg/kg i.p., Sigma, Cat# T5648). After a two-week washout period, breast cancer was induced as previously described [28]. Briefly, a small incision was made to insert a slow-release subcutaneous medroxyprogesterone acetate (MPA) pellet (50 mg, 90-day release, Innovative Research of America, Cat# NP-161) under the skin of the neck. One week after the implant, two cycles of three weekly gavages with dimethylbenzanthracene (DMBA, 1 mg, p.o., Sigma, Cat# D3254) were performed over the next 7 weeks. Starting from the second cycle, mice were palped manually three times per week to detect nodules in the mammary glands. When confirmed, an electronic caliper was used to measure the area of the tumors. Mice were sacrificed when humane endpoint was reached (total area > 1.8 cm^2, ulceration, weight loss > 20% or distress).

Orthotopic breast cancer

0.5×10^6 E0771 cells were resuspended in 100 µL PBS and injected subcutaneously in the fourth left mammary fat pad from syngeneic C57Bl/6J mice (female, 8–10 weeks old) under 3% isoflurane anesthesia. Tumor sizes were measured with an electronic caliper and calculated in mm^2 as $A = \pi/4 \times L \times w$. When the average tumor area became greater than 15 mm^2, mice were randomized into groups of equal tumor sizes to be given either anti-PD1 (BioXCell, clone 29 F.1.A12, 200 µg per mouse i.p. at days 15, 19 and 23 and 27) or the corresponding isotype control (IgG2a, BioXCell, clone 2A3).

ACBP/DBI neutralization

For passive immunization, injections of anti-ACBP/DBI monoclonal antibody [6] or the corresponding isotype control (IgG2a) were administered i.p. at 5 mg/kg, following the schedules presented in the figures. For active immunization, animals were vaccinated against endogenous ACBP/DBI as described [24]. Briefly, recombinant murine ACBP/DBI was conjugated to keyhole limpet hemocyanin (KLH, Thermo Fisher, Cat# 77649) by glutaraldehyde cross-linking at a molar ratio of 20:1. The obtained aqueous solution was mixed 1:1 with the adjuvant Montanide ISA 51VG (Seppic, Cat# 36362/FL2R3) to form an injectable water-in-oil emulsion. The vaccine (KLH-ACBP/DBI or KLH only as a control) was injected *i.p.* once weekly for four consecutive weeks (30 µg, 30 µg, 30 µg and 10 µg, injected in a total volume of 100 µL). After immunization, plasma was collected to check reactivity against ACBP/DBI by immunoblotting.

Carcinogen-induced lung cancer

Six-week-old female C57Bl/6J mice were vaccinated with KLH or KLH coupled to ACBP/DBI. After a two-to-four-weeks washout period, lung cancer was induced by 10 weekly *i.p.* injections of 1 g/kg urethane (Sigma, Cat #U2500) dissolved in 200 µL warm saline (Sigma, Cat# S8776), as described [29]. Mice were euthanized 30 weeks after the first urethane injection, lungs were collected, and macroscopically visible tumors were counted.

Orthotopic NSCLC

0.5×10^6 non-small cell lung carcinoma TC1-Luc were resuspended in 100 µL PBS and injected intravenously into the lateral tail vein of each C57Bl/6J mouse (female, 8–10 weeks old). Tumor development in the lungs was monitored twice per week by bioluminescence imaging to quantify luciferase activity as previously described [30]. Mice were injected i.p. with 150 mg/kg D-luciferin (Promega, Cat# E1605) in 200 µL of PBS. Acquisition was performed on a Xenogen IVIS 50 (Caliper Life Sciences Inc., U.S.A.) 8 min after D-luciferin injection under light anesthesia (2% isoflurane), and the total photon flux was calculated on the region of interest (ROI) around the lungs. The total time of exposure was set at each measurement to avoid saturation: exposure time started with 4 min, and was gradually reduced to 3 min, 2 min, 1 min upon photon saturation. Chemotherapy was started (day 0) five days after tumors were detectable, and mice were randomized by tumor size. Tumor bearing mice showing photon saturation at 1 min of exposure were euthanized. After the end of the measurements, survival was monitored and the mice were sacrificed when reaching humane endpoints (distress, weight loss > 20%).

Skin fibrosarcoma

C57Bl/6J mice (female, 8–10 weeks old) were shaved and injected subcutaneously with 0.3×10^6 MCA205 cells under light isoflurane anesthesia (2% induction for ≤5 min). After 6–7 days, tumors were big enough to be measured by means of an electronic caliper (tumor volume was calculated with the following formula $V=\pi/6\times L\times w\times h$), and mice were randomized to create groups with equivalent tumor burden and body weight repartition [31]. Chemoimmunotherapy was started when tumors reached 50 mm^3 (D0). From this point, tumor size was monitored thrice weekly until one of the following endpoints were reached: tumor larger than 1500 mm^3, ulceration or weight loss > 20% or distress.

Chemoimmunotherapy

At day 0 (see each model for definition), chemoimmunotherapy was initiated with one cycle of oxaliplatin (Sigma, Cat# Y0000271, 10 mg/kg *i.p.*), followed by three cycles of PD-1 neutralizing antibody (BioXCell, clone 29 F.1.A12, 200 µg per mouse *i.p.* at days 8, 12 and 16). Vehicle and isotypes (IgG2a, BioXCell, clone 2A3) were injected following the same route and schedule into the control groups.

Vaccination experiment

On day 0, MCA205-OVA undergoing cell death induced by a 24-hour treatment with 500 µM oxaliplatin (Sigma, Cat# O9512) were collected, rinsed with PBS, and resuspended to a final concentration of 5×10^6 cells/mL. 100 µL of this solution was injected subcutaneously in the lower right back of each mouse two hours after anti-ACBP/DBI or isotype injection (5 mg/kg, i.p.) under light isoflurane anesthesia (Iso-vet isoflurane, 2% induction for ≤5 min). mAb injections were repeated according to the schedule described in Fig. 2. Half the mice were sacrificed at day 6 and the right-side inguinal lymph node was collected sterilely for ex-vivo stimulation. The other half of the mice was rechallenged at day 14 with 0.5×10^6 live MCA205-OVA cells per mouse, also injected subcutaneously. At endpoint (day 20), tumor sizes were measured with an electronic caliper.

Statistics

Longitudinal comparison of the caliper-measured tumor sizes was performed on the online TumGrowth application (https://kroemerlab.shinyapps.io/TumGrowth/). In brief, tumor sizes were modeled by linear mixed effect modeling with treatment and time as fixed affects, and individual mice as random effect. Adequate fitting of the model was verified, and tumor sizes were log-transformed if needed to improve the linear fitting. Type II ANOVA was applied to compare the slopes of tumor size variations with time, and *p*-values were computed using the Wald test with one-sided hypothesis (reduction of slope by the treatment of interest). A factor based on Holm's method was applied to correct for multiple comparisons. For bioluminescence imaging analyses, total flux over same-size ROIs were log-transformed prior to type-II ANOVA on the tumor sizes, and multiple comparisons between treatment groups were corrected with Sidak's method. Survival curves were compared two-by-two by means of the Log-rank Mantel-Cox test.

Immunohistochemistry

For immunohistochemical detection of DBI staining, Bond Leica automated immunostainer instrument was used to perform immunohistochemistry. After fixation of tumors in 4% formaldehyde, 4 µm thick paraffin sections were processed for heat-induced antigen retrieval (Epitope Retrieval Solution 1, corresponding citrate buffer pH = 6, Leica, Cat# AR9961) for 20 min at 100 °C. Slides were incubated with a polyclonal rabbit anti-DBI antibody (Abcam, Cat# ab231910, 1:10000) and with Bond Polymer Refine Detection kit (Leica, Cat# DS9800). The signal was revealed with DAB and counterstained with haematoxylin.

Ex-vivo T cell stimulation

Lymph nodes were passed through a 70 µm strainer and thoroughly rinsed with PBS to obtain single-cell suspensions. Cells were resuspended in serum-free CTL-Test™ medium (Immunospot, Cat# CTLT-010) supplemented with 2 mM L-glutamine, 100 U/mL penicillin and 100 U/

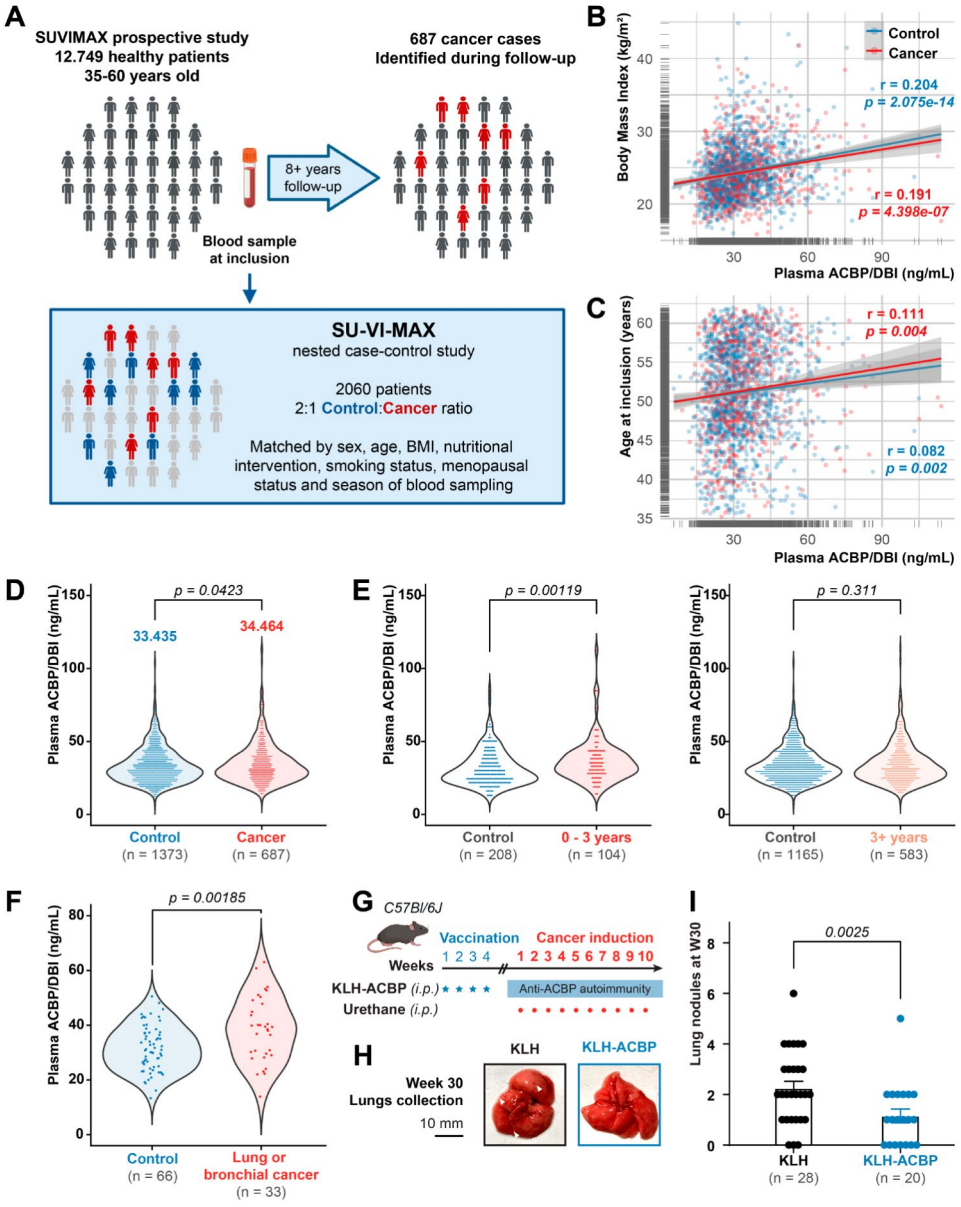

Fig. 2 ACBP/DBI increases in healthy patients prior to (lung) cancer diagnosis. Plasma samples were selected from the inclusion specimens of the 12,749 healthy volunteers enrolled in the SU.VI.MAX study. Each of the 687 patients diagnosed with cancer at any time during follow-up (Cancer group) was matched with two individuals that stayeid disease-free (Control group), controlling for sex, age, body mass index (BMI), nutritional intervention (antioxidants/placebo), smoking status, menopausal status and season of blood sampling (**A**). In both these groups of still-healthy volunteers, population-scale positive Pearson correlations between ACBP/DBI and BMI (**B**) or age (**C**) were observed. The concentration of ACBP/DBI was slightly increased in future cancer patients (**D**). This increase was more pronounced in patients (N = 104) who developed cancer within 3 years after inclusion, but was lost in patients diagnosed at later time points (**E**). Among the most common cancers (N > 20), patients who developed lung cancer ($n = 33$) were the ones with the most prominent increase in ACBP/DBI (**F**). A cohort of mice was vaccinated with four weekly injections of keyhole limpet hemocyanin (KLH) coupled to ACBP/DBI (KLH-ACBP, $n = 20$) or with KLH alone ($n = 28$). After a wash-out period of 2–4 weeks, mice received weekly intraperitoneal injections of urethane (1 g/kg) for 10 weeks (**G**). Lungs were collected 30 weeks after the first urethane injection. Representative images are shown in (**H**) and the number of macroscopic lung tumors was compared between the two experimental groups (**I**). Statistical analyses were performed by one-sided, unpaired Student's t-tests for normally distributed plasma ACBP/DBI measurements and by one-sided Mann Whitney tests for lung nodule counts

mL streptomycin (Gibco) and used for IFN-γ enzyme-linked immunospot (ELISPOT) following the manufacturer's instructions (Mabtech, Cat# 3321-4APT-2). Briefly, 0.5×10^6 cells were seeded in each well of a 96-well PVDF ELISPOT plate pre-coated with anti-murine IFN-γ antibody (clone AN18). Each biological sample was tested in unstimulated condition (medium only) and either dominant MHC-I-restricted (SIINFEKL, 2 µg/mL) or MHC-II-restricted (ISQAVHAAHAEINEAGR, 2 µg/mL) OVA peptides for 16 h. Wells were rinsed

thoroughly and IFN-γ signal was revealed with a biotinylated IFN-γ-reactive detection mAb (clone R4-6A2), streptavidin-ALP and BCIP-NBT plus enzymatic substrate. Spot counts were performed automatically on the Immunospot software (ISQAVHAAHAEINEAGR and unstimulated groups) or on ImageJ when the number of dots was high (SIINFEKL group). Visual inspection of the spots masks confirmed that the sensitivity of spots detection was comparable within each group (Fig. S5D). The specific spot count for each peptide was defined as $\max(0, N_{SPOTS,\ PEPTIDE} - N_{SPOTS,\ UNSTIMULATED})$ and statistically compared by non-parametric, one-tailed Mann-Whitney test.

Flow cytometry analysis of the immune infiltrate

At day 10, MCA205-bearing mice were euthanized and tumors were collected and dissociated to a single cell suspension by mechanical and enzymatic disruption, following the manufacturer's instruction (tumor dissociation kit, Miltenyi Biotec, Cat# 130-096-730). Cells were stained with a viability staining (Live-Dead Fixable Yellow Dye, Invitrogen, Cat# L34967) then Fc receptors were blocked by an uncoupled anti-mouse CD16/CD32 antibody (BD BioSciences, clone 2.4G2) and fluorophore-coupled antibodies were added for the detection of surface markers (CD45-BUV661, RRID: AB_2870247, CD3-APC, RRID: AB_10597589, CD4-APC-Vio770, RRID: AB_2751634, CD8a-PE, RRID: AB_394570, ICOS-BV421, RRID: AB_2738576, GITR-BV786, RRID: AB_2740641, LAG3-BV605, RRID: AB_2742805, PD1-BUV395, RRID: AB_2742320, TIGIT-BV711, RRID: AB_2742063 and VISTA-PerCP-Cy5.5, RRID: AB_2561400). Cells were fixed and permeabilized (eBioscience FoxP3/Transcription Factor staining buffer, Thermo Fisher, Cat# 00-5523-00) prior to intranuclear staining (FoxP3-FITC, RRID: AB_465243). Fluorescence data were acquired on a BD LSRFortessa X20 with the BD FACS Diva software. Compensation, scaling, gating and data analysis were performed on the omiq.ai online platform. In addition to the classical cell populations, specific subpopulations of interest were defined among $CD4^+$ and $CD8^+$ T cells by performing unsupervised clustering in one of the three independent experiments. More specifically, the opt-SNE algorithm was used to perform dimension reduction, and then the FlowSOM algorithm was applied to split the clusters. Gating strategies were inferred from the markers expressed by the clusters of interest (differentially present between the CT+anti-PD1 and anti-ACBP/DBI+CT+anti-PD1) and applied to the pooled data from three independent experiments for statistical analysis (Figure S6). Statistical comparison was performed on pooled data from all experiments, after elimination of the outliers (ROUT test, Q=1%), by one-way ANOVA with Sidak's correction for multiple comparisons.

Single-cell RNA sequencing of the intratumoral T cell populations

Sample preparation

MCA205 tumors were collected and homogenized following the same protocol as the one used for flow cytometry. The single-cell suspension was incubated in anti-mouse CD16/CD32 antibody (BD Biosciences, Cat# 553142, RRID: AB_394656), then stained with a fluorescent mix of 4',6-diamidino-2-phénylindole (DAPI, viability) and fluorescent-labelled antibodies. T cells were sorted on a BD Aria III as the cells that were negative for all lineage markers (CD11c, RRID: AB_647251, Ly6C, RRID: AB_1727557, Ly6G, RRID: AB_1877261, F4/80, RRID: AB_2733261, NK1.1, RRID: AB_394507, CD19, RRID: AB_394495, all in the PE-Cy7 channel) and positive for CD45(-AF488, RRID: AB_493531) and either CD4(-PerCp-Cy5.5, RRID: AB_1107001) or CD8(-PE, RRID: AB_394571). After sorting, cells were counted and resuspended at a ratio of 1 $CD4^+$ to 1 $CD8^+$ T cell before loading a total of 10,000 cells to the Chromium Next GEM Chip K for emulsion. All subsequent steps, including retro-transcription, cleanup, cDNA amplification and libraries construction, were performed according to the Single cell 5' VDJ v2 manufacturer's instruction (10× Genomics, USA). Libraries were sequenced on Illumina NovaSeq 6000, with paired-end 150 bp and 28/90 bp runs for gene expression and T cell receptor sequencing.

Data pre-processing

Single-cell 5' and V(D)J data analyses was performed by GenoSplice technology (www.genosplice.com). Sequencing data quality was assessed using FastQC v0.11.5 on 6 mouse expression and VDJ samples. For read alignment, unique molecular identifiers (UMI) quantification and paired clonotype calling, the CellRanger software v7.0.0 was used on Mus Musculus 2020 A reference (genome mm10, gene annotation Ensembl 98 and VDJ reference) with default parameters. Cellranger multi and aggregate function were used. The 6 expression matrices containing the UMI counts were merged, and only the genes with UMI≥1 in at least one cell were kept. The following filters were applied to generate a global matrix used in further analysis: cells with UMI≥1300, number of detected genes≥800, and cells with UMI in mitochondrial genes≤10%. In order to estimate and suppress ambient RNA, DecontX (Yang et al., 2020) R package was applied on counts data from cellranger. DoubletFinder (McGinnis, Murrow, & Gartner, 2019) with 10x expected percentage of doublets was used to suppress doublets (8% for C1, C2, D1 and D3, 7.60% for C3 and 6.09% for

D2). Single-cell 5′ and V(D)J were integrated in a Seurat object.

Clustering

For normalization and clustering, Seurat 4.0.3 was used [32] and SCTransform normalization was applied. To avoid bias due to Tcell receptor genes, all Trav/Traj/Trbc/Trbv genes were suppressed from variable genes. Based on elbow plot, 31 PC were used for UMAP calculation and clustering analysis. Clustering step was performed using default parameters from Seurat (FindNeighbors and FindClusters functions). To calculate markers for each cluster, a global-scaling normalization method was applied with a scale factor of 10,000 and log-transformation of data. Only genes expressed in at least 25% of cells with a log2FC minimum of 0.25 an adjusted p-value inferior at 0.05 were considered as markers using Seurat Wilcoxon test. Based on a treemap of clusters with different resolution parameters and clusters markers, we chose a resolution parameter of 0.2. Low-frequencies clusters without *Cd3g/d/e* expression, which resulted from sorting approximations, were excluded for downstream analysis (clusters 9 and 11). Cluster 5 was also excluded due to low UMI count, and the remaining 9 clusters were numbered from 0 to 8 (largest to smallest number of cells).

Statistics

Differentially expressed genes (DEG) analysis was performed in each cluster using a Wilcoxon test from Seurat, genes expressed in at least 25% of cells in one condition, with a log2FC minimum of 0.25 an adjusted p-value inferior at 0.05 were considered. Single cell pseudo-time trajectory analysis was performed with monocle3 [33] independently on $CD4^+$ cells and $CD8^+$ cells. Root was defined based on a clear expression pattern of the naïve T -cells markers *Sell*, *Ccr7* and *Tcf7*. Differences between cluster compositions were compared by chi-square test.

Results

Elevated ACBP/DBI levels in cancer predisposition syndromes

Li-Fraumeni syndrome is caused by a deleterious germline *TP53* alteration and characterized by the early (<45 years) manifestation of sarcomas and other cancers, often in the context of a family history of neoplastic disease [34]. We measured plasma levels of ACBP/DBI in a cohort of clinically cancer-free patients recruited in the LIFSCREEN prospective trial (NCT01464086). All participants were carriers of germline pathogenic or likely pathogenic variants in the *TP53* gene (*gTP53m*). When comparing them with age, BMI and sex-matched healthy controls from the DESIR cohort [9] (2 controls per case, Fig. 1A, Table S1), we found that plasma ACBP/DBI concentrations were higher in *gTP53m* patients than in controls (Fig. 1B). We found a significant (Spearman) positive correlation between ACBP/DBI and BMI and age in healthy controls that was lost (for BMI) or inverted (for age) in *gTP53m* patients (Fig. S1). In this series, elevated ACBP/DBI concentrations predicted the *gTP53m* status associated with high sensitivity and specificity (area under the curve [AUC] of the receiver operator curve [ROC]=0.948, Fig. S1). We also found elevated plasma ACBP/DBI levels in $Trp53^{-/-}$ mice (*Trp53* is the mouse orthologue of human *TP53*), but no changes in mice overexpressing transgenic *Trp53* (Fig. 1C, D). Short-term inhibition of p53 by pifithrin-α injection did not cause an increase in plasma ACBP/DBI, contrasting with the effect of pro-inflammatory lipopolysaccharide, which causes a surge in ACBP/DBI (Fig. 1E). This suggests that ACBP/DBI is not under the direct transcriptional repression of TP53/p53, in accord with our prior observations [35], but rather indicates that the long term-effects of *TP53*/*Trp53* deficiency, which affect metabolism and inflammation [34, 36], cause an increase in ACBP/DBI.

We also observed high plasma ACBP/DBI concentrations in women carrying germline mutations in *BRCA1* or *BRCA2*, which both predispose to the development of breast cancer, compared to age-matched controls (Fig. 1F, G). Of note, female mice subjected to knockout of *Dbi* (Fig. S1G) developed less aggressive cancers than control mice in a model of hormone-driven mammary carcinogenesis, suggesting a pathogenic role for ACBP/DBI in breast cancer progression (Fig. 1H, I, S1H, I). ACBP/DBI inactivation specifically extended the post-diagnosis survival (Fig. 1I), which has been demonstrated to be under the control of inteferon-γ (IFNγ) producing T cells [28]. Accordingly, in mice bearing orthotopic E0771 breast cancers, neutralization of ACBP/DBI by repeated intraperitoneal injections of a monoclonal antibody (mAb) combined with PD-1 checkpoint blockade, but neither of the two treatments alone, prolonged survival and reduced tumor growth (Fig. 1J-L, S1J-L).

In conclusion, it appears that ACBP/DBI plasma levels are elevated in two cancer predisposition syndromes, namely *TP53* and *BRCA1/2* mutations. Moreover, in mouse models of breast cancer, ACBP/DBI neutralization slows down breast cancer progression, especially in the context of PD-1 blockade.

Prediagnostic elevation of ACBP/DBI levels in individuals at risk of lung cancer

Next, we investigated the potential predictiveness of high ACBP/DBI concentrations as a biomarker of future cancer diagnosis in the SU.VI.MAX cohort, a population of healthy individuals who donated blood samples from 1994 and enrolled in a clinical follow-up of ≥8 years [22]. In this cohort of 12.749 individuals, 687 were diagnosed

with cancer. We matched these 687 cases with cancer-free controls (2 controls per case) by sex, age, BMI, nutritional intervention, smoking and menopausal status, as well as the season of blood sampling (Fig. 2A, Table S3). Both cases and controls exhibited a positive correlation between plasma ACBP/DBI and BMI (Fig. 2B) and age (Fig. 2C). The plasma ACBP/DBI concentrations were slightly (but significantly) higher in future cancer patients than in their matched controls (Fig. 2D). This difference was more pronounced in patients with imminent (within 3 years) cancer diagnosis after blood sampling compared to their time-matched controls but vanished for patients developing cancer after >3 years (Fig. 2E). Statistical analyses of ACBP/DBI levels according to the most frequent cancer types (>20 cases in the cohort, Fig. S2) revealed particularly high ACBP/DBI levels before the diagnosis of lung cancer (Fig. 2F). While the AUC of high plasma ACBP/DBI as a predictor of the diagnosis of cancer within 3 years was 0.625 (Fig. S2B), the AUC for the diagnosis of lung cancer at any time point was 0.680 (Fig. S2C).

To study the effects of ACBP/DBI on lung carcinogenesis in a preclinical model, mice were vaccinated with the immunostimulant protein keyhole limpet hemocyanin (KLH) alone as a control, or a KLH-ACBP/DBI conjugate (KLH-ACBP), which induces anti-ACBP/DBI autoantibodies [24]. These mice were then chronically exposed to urethane, a carcinogenic carbamate that induces lung cancers that are under T cell-dependent immunosurveillance [29, 37] (Fig. 3G, H). The KLH-ACBP vaccine reduced the number of lung tumors compared to KLH controls (Fig. 3I).

In conclusion, it appears that ACBP/DBI plasma levels are higher in non-syndromic patients announcing imminent cancer diagnosis, in particular that of lung cancer. In mice, ACBP/DBI neutralization reduces chemically induced lung carcinogenesis.

Effects of ACBP/DBI on lung cancer immunosurveillance

Pretreatment of mice with an mAb neutralizing extracellular ACBP/DBI [6] reduced non-small cell lung cancer (NSCLC) development in two models: one in which mice were challenged subcutaneously with TC1 NSCLC cells (Fig. S3A), and a second one in which TC1 cells expressing luciferase were injected intravenously (i.v.) into the tail vein (Fig. 3). Such cells then seed into the lung to form orthotopic NSCLC [30] (3A). Tumors monitored by bioluminescence imaging [30] (Fig. 3B) progressed less vigorously after intraperitoneal (*i.p.*) pretreatment with anti-ACBP/DBI mAb than in controls injected with an irrelevant isotype control mAb (Fig. 4B, C; Fig. S3B). Of note, orthotopic luciferase-expressing TC1 cancers progressed at an equal pace in athymic nude mice, which lack thymus-derived T cells, irrespective of the treatment with anti-ACBP/DBI mAb (Fig. 3D, E). Thus, the tumor growth-reducing effect of the ACBP/DBI antibody alone must rely on T cell-mediated cancer immunosurveillance. To investigate the impact of ACBP/DBI on therapy-induced immunosurveillance, we treated NSCLC-bearing mice with anti-ACBP/DBI mAb together with a synergistic chemoimmunotherapy regimen involving oxaliplatin and PD-1 blockade [38] (Fig. 3F, G). The combination of anti-ACBP/DBI mAb and chemoimmunotherapy reduced tumor progression (in 17/21 mice) and increased survival beyond 60 days (in 13/21 mice) compared to isotype control-injected mice that always developed rapidly expanding tumors (Fig. 3H, I).

In sum, these results suggest that ACBP/DBI subverts immunosurveillance of NSCLC, notably in the context of chemoimmunotherapy.

Enhanced anticancer T cell response upon ACBP/DBI neutralization

Next, we switched to another orthotopic cancer model, namely, cutaneous fibrosarcoma MCA205 tumors implanted in mice that were subjected to ACBP/DBI neutralization by active or passive vaccination. Subcutaneous MCA205 tumors responded more efficiently to chemoimmunotherapy in mice that had been vaccinated with KLH-ACBP/DBI [24] (Fig. S4G) as compared to mice that had been vaccinated with KLH alone (Fig. S4D-I). Similarly, repeated i.p. injections of the anti-ACBP/DBI mAb led to superior outcome of chemoimmunotherapy compared to isotype control mAb injections (Fig. 4A-C, Fig. S4G, H). We conclude that, in preclinical models, ACBP/DBI neutralization boosts the efficacy of chemoimmunotherapy against both NSCLC and sarcoma.

In response to vaccination with chemotherapy-treated MCA205 cells that were engineered to express the model antigen ovalbumin (OVA), T cell responses against dominant MHC class-I and MHC class-II-restricted OVA-derived peptides were enhanced by ACBP/DBI neutralization at the level of IFNγ secretion (Fig. 4D,E, Fig. S4J-L). Moreover, at the functional level, after vaccination with dying OVA-expressing MCA205 cells, the control of sarcomas arising from rechallenge with live cells was improved by anti-ACBP/DBI mAb (Fig. 5G, H).

Altogether these results suggest that neutralization of ACBP/DBI stimulates T cell-mediated anticancer immunosurveillance.

Mechanisms of the immunostimulatory action of ACBP/DBI neutralization

To elucidate the immunostimulatory mechanisms of ACBP/DBI neutralization, we implanted MCA205 sarcomas orthotopically (under the skin) of immunocompetent mice and subjected them to combinations of chemotherapy, PD-1 blockade and ACBP/DBI neutralization in

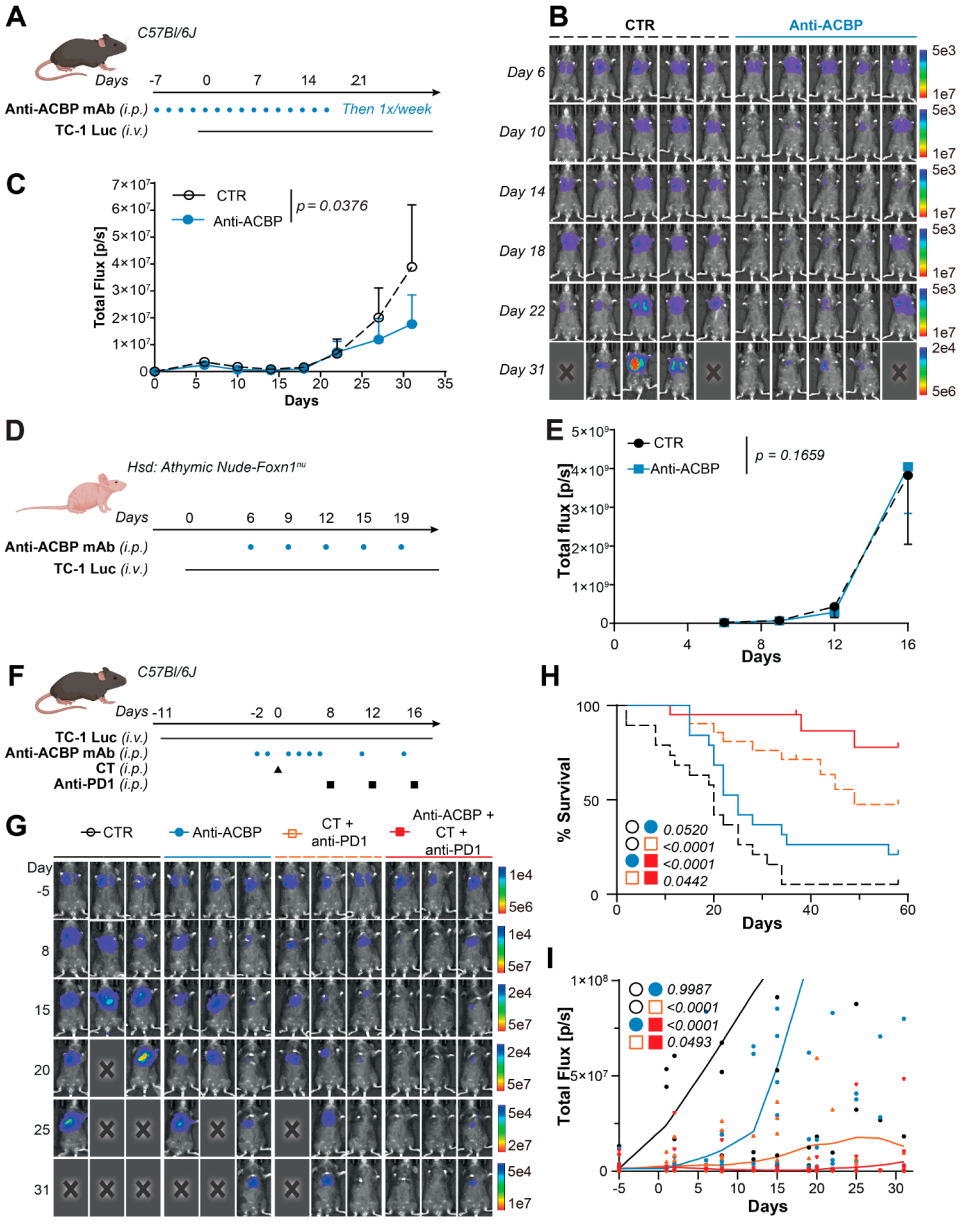

Fig. 3 ACBP/DBI neutralization improves immunosurveillance of NSCLC in mice. Anti-ACBP/DBI mAb or isotype-matched control mAb was repeatedly injected intraperitoneally (i.p.), starting two days before intravenous (i.v.) injection of TC1 NSCLC cells expressing luciferase (TC1-Luc) into immunocompetent C57Bl/6 mice (**A**). Anti-ACBP/DBI mAb reduced the progression of orthotopic NSCLC cancers developing in the thoracic cage, as determined by chemoluminescence imaging (**B**, **C**). Alternatively, ACBP/DBI neutralization was performed in immunodeficient Hsd:Athymic Nude-Foxn1nu mice starting from tumor detection (**D**). Repeated injections of anti-ACBP/DBI mAb failed to slow down tumor progression in these athymic animals (**E**). In immunocompetent C57Bl/6 mice bearing orthotopic NSCLC (TC1-Luc), neutralization of ACBP/DBI was achieved by recurrent injections of monoclonal antibody (mAb) during chemoimmunotherapy (CT + anti-PD1), following the schedule (**F**). Tumor growth was monitored in situ by bioluminescent imaging (**G**). ACBP/DBI neutralization improved mouse survival both with and without chemoimmunotherapy (H) by slowing down tumor growth (**I**). Individual longitudinal tumor growth curves from two independent experiments are displayed in the background, the group tendencies are represented by locally weighted scatterplot smoothing curves (5 points per smoothing window). Statistical comparisons were performed by log-rank (Mantel-Cox) tests for survival and by 2-way ANOVA after log-transformation for tumor bioluminescence

short-term experiments in which the size of the tumors was comparable at endpoint (Fig. 2F), two days after one single cycle of immunotherapy (Fig. 5A). High-dimensional immunofluorescence cytometry (for gating strategy see Fig. S5AB) allowed to detect major shifts in tumor-infiltrating T lymphocyte subpopulations (Fig. 5B-K) but no major alterations in myeloid cells (Fig. S5C).

The combination treatment (chemoimmunotherapy + ACBP/DBI blockade) was more efficient than each treatment modality alone (chemoimmunotherapy or

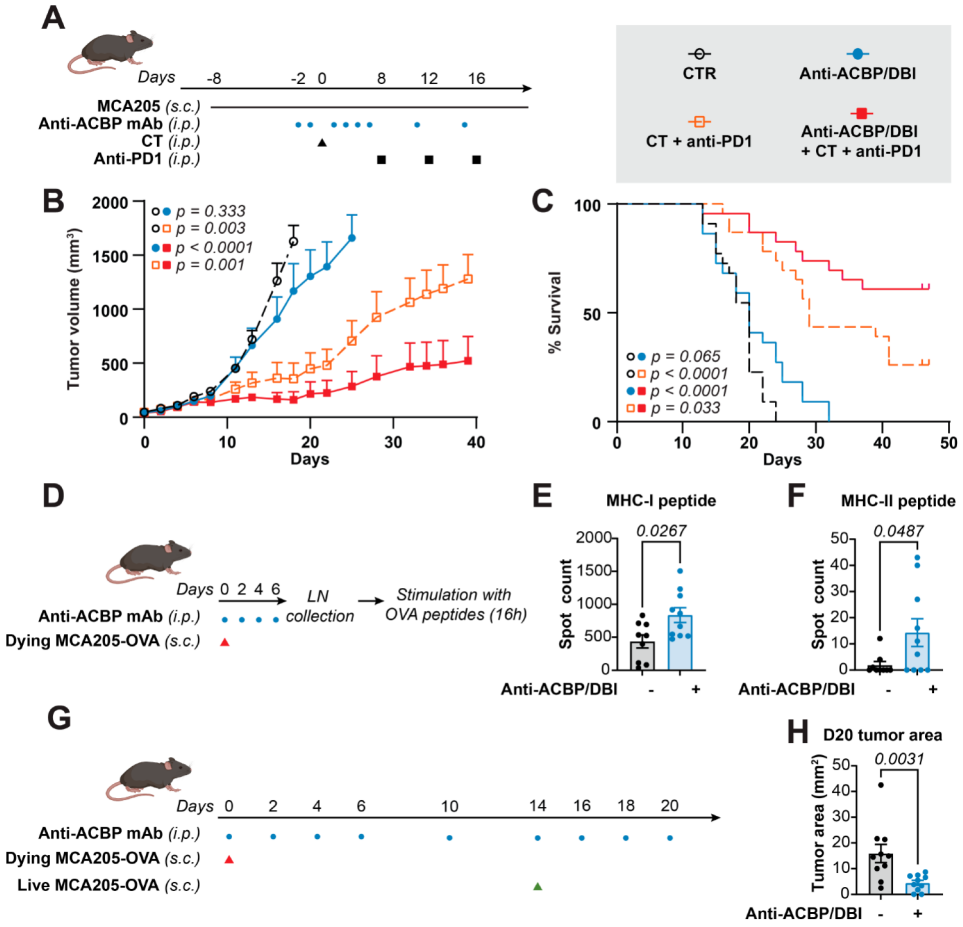

Fig. 4 ACBP/DBI neutralization improves immune responses against tumor antigens. Mice bearing MCA205 skin fibrosarcoma were treated with chemoimmunotherapy (oxaliplatin plus PD-1 blockade) alone or in combination with ACBP/DBI neutralization (A), which slowed tumor growth (B) and prolonged survival (C). The immune response against tumor antigens was tested by subcutaneous injection of MCA205 expressing ZsGreen fluorescent protein coupled to ovalbumin (OVA) after in vitro treatment by chemotherapy (oxaliplatin), with concomitant intraperitoneal injections of ACBP/DBI-neutralizing mAb or its isotype (5 mg/kg) (D). Six days after the injection of such dying tumor cells, the draining lymph nodes were collected and stimulated with the major histocompatibility complex-I (MHC-I)-dominant (SIINFEKL) or MHC-II-dominant (ISQAVHAAHAEINEAGR) OVA peptides to quantify interferon-γ (IFN-γ)-producing T cell clones by ELISPOT (E,F). The same experimental setup was repeated and followed by the injection of live MCA205-OVA tumor cells two weeks after the first challenge (G) and measurement of tumor size at day 20 (N). Tumor growth curves were compared by linear mixed effect modeling on the https://kroemerlab.shinyapps.io/TumGrowth/ platform. Survival was tested by log-rank (Mantel-Cox) test. In the vaccination experiments, the number of spots per biological replicate were compared by one-sided Mann-Whitney rank test and the endpoint tumor sizes by one-sided Student's t-test

ACBP/DBI blockade) in increasing infiltration by cytotoxic T lymphocytes (CTL, defined as $CD3^+CD8^+$) and T helper cells (T_H, defined as $CD3^+CD4^+Foxp3^-$), but decreasing regulatory T cells (T_{REG}, defined as $CD3^+CD4^+Foxp3^+$), hence improving the CTL/T_{REG} and CTL/ T_H ratios (Fig. 5B-I). Moreover, the combination treatment stood out for reducing the frequency of CTL and T_H expressing the exhaustion marker LAG3 (Fig. 5J, K). Non-supervised clustering of $CD4^+$ and $CD8^+$ T cells by means of the opt-SNE method based on 8 activation/exhaustion markers allowed to identify multiple subpopulations (Fig. 5L, M). The comparison of cluster distribution between tumors from mice undergoing chemoimmunotherapy alone or in combination with ACBP/DBI blockade (Fig. 5M, N) revealed an absolute depletion of T_{REG} cells with a non-exhausted $ICOS^+GITR^+Lag3^-$ phenotype (Fig. 5O) and an expansion of T_H with an activated $ICOS^{med}$ $GITR^+$ $Lag3^-$ $PD1^-$ phenotype (Fig. 5P). Other exhaustion markers than LAG3 (ICOS, GIT4, TIM3, TIGIT, PD1 and VISTA) were particularly abundant in $CD4^+$ subset Q and in $CD8^+$ subsets d and c (Fig. 5M, upper panel). Among these subpopulations, only $CD8^+$ subset d was significantly reduced by anti-ACBP/DBI antibody (Fig. 5M, lower panel).

To further characterize the ACBP/DBI effects on the cancer immune infiltrate, we used a similar experimental setting as above (though restricted to only two groups: chemoimmunotherapy alone or in combination with

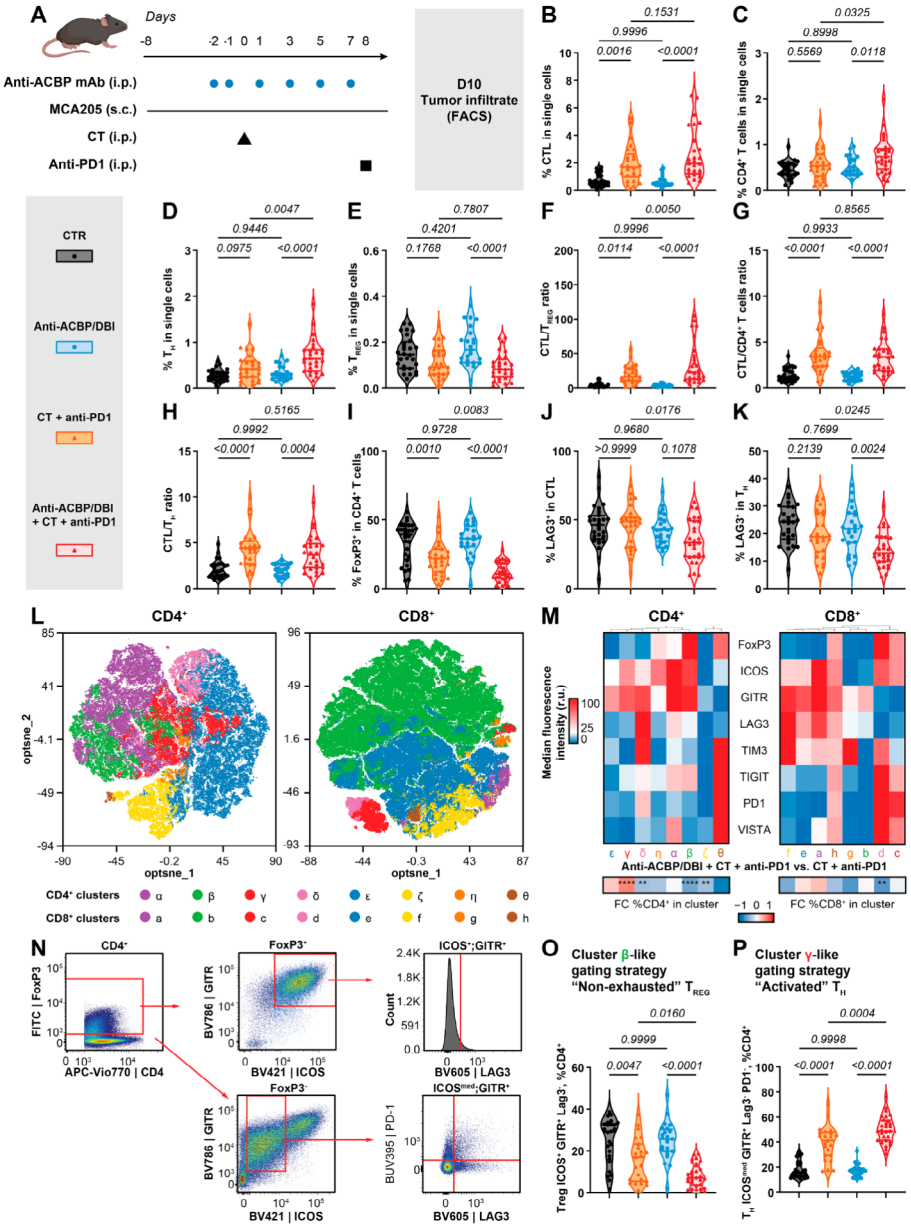

Fig. 5 ACBP/DBI-neutralization improves the immune control of MCA205 carcinomas during chemoimmunotherapy. T cell populations of the tumor microenvironment were analyzed by flow cytometry eight days after the beginning of chemoimmunotherapy (consisting of one cycle of chemotherapy, CT, and one cycle of immune checkpoint blockade, anti-PD1, **A**). The number of specific cell populations relative to the total analyzed single cells is presented for cytotoxic T lymphocytes (CTL, $CD3^+CD8^+$, **B**) and $CD4^+$ T lymphocytes (**C**). Within the $CD4^+$ population, $CD4^+$, $FoxP3^-$ helper T cells (T_H, **D**) and $CD4^+$, $FoxP3^+$ regulatory T cells (T_{REG}, **E**) were analyzed separately. The good-prognosis ratios between the counts of CTL and T_{REG} was increased by anti-ACBP/DBI injections in the context of chemoimmunotherapy (**F**), while this was not the case for the CTL/$CD4^+$ (**G**) or CTL/T_H ratios (**H**), indicating an increase in cancer-directed cytotoxicity. The percentage of $CD4^+$ T cells that were immunoregulatory ($FoxP3^+$) was decreased (**I**). Finally, the proportion of CTL (**J**) and T_H (**K**) cells expressing the exhaustion marker LAG3 decreased with the combination therapy. Unsupervised clustering was applied to $CD4^+$ and $CD8^+$ T cells subsets on 8 phenotypic markers: the FoxP3 nuclear factor, two costimulatory surface receptors (inducible T cell costimulator, ICOS; glucocorticoid-induced TNFR-related protein, GITR) and five early-to-late exhaustion surface markers (lymphocyte activation gene-3, LAG3; T cell immunoglobulin and mucin containing protein-3, TIM3; T cell immunoreceptor with Ig and ITIM domains: TIGIT; Programmed cell death protein 1, PD1; and V-domain Ig suppressor of T cell activation, VISTA). Eight populations were defined within the $CD4^+$ (α-θ) and $CD8^+$ (**a-h**) cells (**L**), and the median fluorescence of each marker is represented as a heatmap (**M**). The relative abundance of these eight clusters was compared between chemoimmunotherapy alone or in combination with ACBP/DBI neutralization by Chi2 test and represented as fold-change (**M**). Manual gating was applied to recapitulate features of the two most differentially abundant clusters (**N**): the β-like cluster of T_{REG} ($CD4^+$;$FoxP3^+$;$GITR^+$;$Lag3^-$, O) and the γ-like cluster of T_H ($CD4^+$;$FoxP3^-$;$ICOS^{med}$;GITR$^+$;Lag3-, P), which were depleted and increased, respectively, by the combination therapy. Compensation, scaling and gating strategies were performed using the omiq.ai platform. Data from three independent experiments are presented, population relative counts were cleaned up by ROUT test (outlier threshold = 1%), and *p*-values were calculated by one-way ANOVA with Sidak's correction for multiple comparisons

ACBP/DBI blockade) and performed single-cell RNA-seq (scRNAseq) analyses of purified $CD4^+$ and $CD8^+$ T cells (at a 1:1 ratio). This procedure identified 9 major T cell subpopulations (Fig. 6A, B), with significant shifts between the two groups. Thus, anti-ACBP/DBI mAb reduced the frequency of T_{REG} cells (cluster 2) and elevated that of CTL (clusters 0, 3, 6) (Fig. 6C), confirming the results obtained by immunofluorescence cytometry (Fig. 5). More detailed analyses of the abundance of specific mRNAs revealed an ACBP/DBI neutralization associated increase in CTL effector molecules (e.g. *Gzmb*, *Nkg7*), a decrease in inhibitory immune checkpoint molecules (*Pdcd1*/PD-1, *Ctla4*) and an increase in stimulatory immune checkpoint markers (*Icos*, *Cd28*) on a per-cell basis across several T cell clusters (Fig. 6D). Computation of pseudo-time trajectories suggested a decreased propensity of $CD4^+$ T cells to adopt an exhausted or regulatory end-stage phenotype in absence of ACBP/DBI blockade (Fig. 6E). In contrast, the most important shifts in $CD8^+$ T cells induced by ACBP/DBI blockade appear to occur within cluster 0 at early stage (Fig. 6F). Differential gene expression analyses unveiled effect of ACBP/DBI blockade that affected each of the clusters, alone, or in combination (Fig. S6, Table S4). Of note, 5 genes (*Gadd45b*, *Lmna*, *Lgals3*, *Ubc*, *Csf1*), were found to be upregulated in all ($CD4^+$ or $CD8^+$) T cell clusters. Among these genes, *Lmna*, which encodes for Lamin A/C, an obligatory T cell activation marker [39, 40], stood out for being upregulated by all T cell clusters (Fig. 6G, Fig. S6).

In sum, the immunophenotypic and transcriptomic analysis of tumor-infiltrating T lymphocytes provides a congruent demonstration that ACBP/DBI blockade augments T cell activation in all T cell subpopulations, improves CTL effector functions, but blunts TREG activity and reduces the expression of major inhibitory immune checkpoints.

Discussion

Although cancer research has been focusing until recently on (epi)genetic alterations in (pre-)malignant cells to understand oncogenesis and tumor progression, it has become clear over the last decade that extra-tumoral factors including aging, whole-body metabolism and (neuro-)endocrine factors play a major role in determining the trajectory of malignant diseases [41–43]. In the present paper, we describe that ACBP/DBI might be an important determinant in the ecosystem that influences cancer formation and progression. Indeed, ACBP/DBI has a pro-aging effect and increases with age [8, 9], which is arguably the most important risk factor for neoplasia [44]. ACBP/DBI also increases with BMI [6, 8], independently of age [7, 8], knowing that obesity is among the most important modifiable risk factors of cancer [45]. Here, we show that, independently of age and BMI, an elevation of ACBP/DBI is associated with increased risk to develop cancer. As a possible interpretation, this might indicate that as a potential biomarker of (premature) biological aging, elevations of ACBP/DBI reflect a general (patho)physiological stage that is prone to cancerization.

In our cohort, before the diagnosis of a new cancer, patients with *gTP53m* had increased levels of ACBP/DBI plasma concentrations as compared to controls. The same applied to patients with *BRCA1/2* mutations. Moreover, in non-syndromic, apparently healthy participants that volunteered to be enrolled in a trial evaluating dietary supplements (revealing no overall effects of antioxidant preparations) [21, 22], ACBP/DBI plasma levels were elevated before the development of malignant disease, especially if cancer diagnosis was imminent (≤3 years) or when the yet-to-be-discovered neoplasia affects the lung. Both sarcomas (part of the core spectrum of the Li-Fraumeni syndrome) [46] and NSCLC (which is the most frequent carcinoma affecting the bronchial tract and frequent in *gTP53m* carriers) are known to be under strong immunosurveillance [47, 48], meaning that they can only develop after escaping immune recognition. Moreover, even advanced NSCLC can be successfully delayed in its progression with immunotherapy, often in a neo-adjuvant setting in combination with chemotherapy [49]. This suggests that cancer cell-extrinsic factors such as ACBP/DBI (measured in the plasma) might modulate immunosurveillance to affect the onset of malignant disease as well as treatment responses.

Previous studies have suggested that ACBP/DBI expressed by NSCLC cells contributes to disease pathogenesis. Thus, ACBP/DBI mRNA levels are overabundant in NSCLC, correlating with poor prognosis and tumor stage [16]. Knockdown of ACBP/DBI reduced NSCLC proliferation in cell culture, suggesting a cell-autonomous effect [16]. Here, we found that high extracellular (plasma) levels of ACBP/DBI predicted future NSCLC diagnosis and that neutralization of extracellular ACBP/DBI (by means of neutralizing antibodies) reduced NSCLC progression in preclinical models. Although, we cannot exclude that the intra- and extra-cellular pools of ACBP/DBI are connected to each other, it appears improbable that mAb-mediated ACBP/DBI neutralization has a direct effect on NSCLC cells because the anti-NSCLC effect was only observable in the presence of an intact immune system.

ACBP/DBI reportedly increases in a variety of pro-inflammatory conditions including diabetes [50], steatohepatitis [51], osteoarthritis [52], infection by human immunodeficiency virus (HIV) [53], severe COVID-19 [54], as well as surgery complicated by inflammation [55]. Mouse experimentation indicates that ACBP/DBI neutralization has strong anti-inflammatory effects, hence dampening the activation of the inflammasome

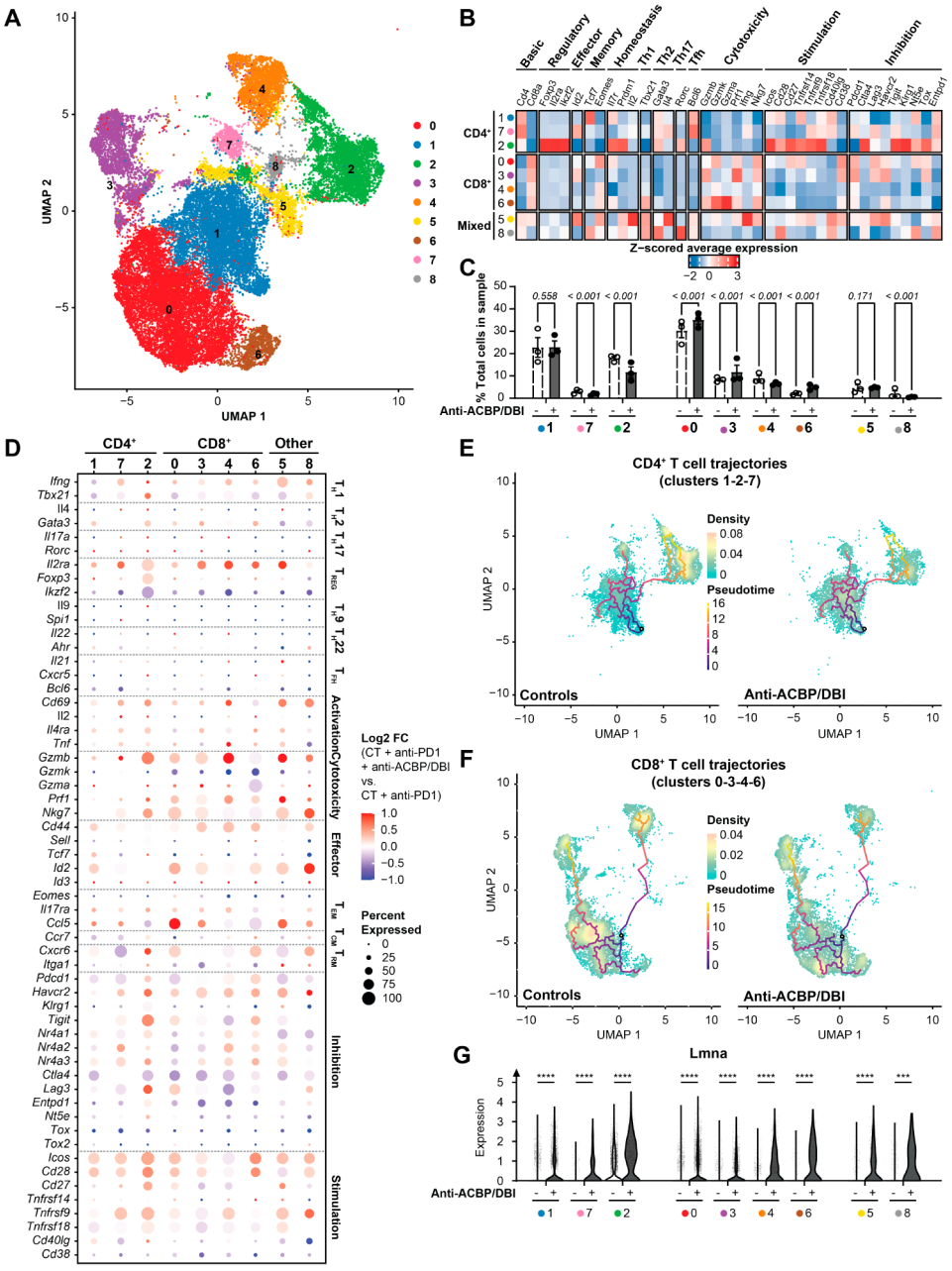

Fig. 6 Single-cell RNA sequencing of the T cell immune infiltrate. Uniform manifold approximation and projection (UMAP) represents the 9 clusters of T cells infiltrating the MCA205 tumors 10 days after the beginning of chemoimmunotherapy (CT + anti-PD1), with or without ACBP/DBI-neutralizing monoclonal antibody (anti-ACBP/DBI) (**A**). Three CD4$^+$ (1, 2 and 7) and four CD8$^+$ main clusters (0, 3, 4 and 6) were identified based on their top differentially expressed genes and the expression of typical phenotypic genes, plotted as a heatmap of Z-score average expression per cluster (**B**). The remaining two clusters [5, 8] were constituted of mixed populations of CD4$^+$ and CD8$^+$ T cells. The repartition of cells per cluster in each sample was different between anti-ACBP/DBI-treated and isotype-treated samples, as tested by Chi2 test (**C**). Within each cluster, the phenotypic changes induced by anti-ACBP/DBI treatment were represented as a dot plot (**D**). In this graph, dot sizes represent the percentage of cells expressing the gene in the cluster, and colors indicate the log2 fold-change of gene expression between conditions. A Monocle3 trajectory analysis of the CD4$^+$ (**E**) and CD8$^+$ T cells (**F**) unveiled differential accumulation of the T cells along the trajectory between conditions, with less cells at the terminal side of the trajectories in anti-ACBP/DBI treated samples. Cells are represented as dots and colored based on local density, and the trajectory (starting on the white dot and colored by pseudo-time) is overlaid on the UMAP projection. The essential T cell activation gene *Lmna* (coding for lamin A/C) was overexpressed in all clusters, as pictured on the violin plot (**G**). Expression data were log2-normalized by cluster and condition, and *p*-values were computed by Wilcoxon test between the two conditions in each cluster

and the production of inflammatory cytokines including interleukin(IL)-1b (IL1b) and IL6 [15]. Inflammation is well known to contribute to the development of clinically detectable NSCLC as indicated by the disease-preventive effects of canakinumab, an IL-1b -neutralizing antibody in patients with cardiovascular disease [56]. Hence, one possible explanation for the positive effects of ACBP/DBI neutralization on mouse NSCLC might be the suppression of pathogenic inflammation, which is immunosuppressive.

Beyond these speculative aspects, in the MCA205 skin sarcoma model, it appears clear that ACBP/DBI neutralization boosts anticancer immune responses in the context of chemoimmunotherapy, hence improving tumor growth control and shifting the immune infiltrate, especially at the level of T lymphocyte subpopulations. Among the most spectacular changes are a relative decrease in the abundance of T_{REG} cells (as compared to CTL or T_H cells), improved CTL effector functions (as suggested by the upregulation of components of cytotoxic granules) and reduced expression of major inhibitory immune checkpoints (CTLA-4, LAG-3, PD-1) on most T cell subpopulations. Among the most salient effects of ACBP/DBI blockade appears the upregulation of the mRNA coding for lamin A/C, which is a marker of T cell activation [40], and indispensable for this activation to occur because its genetic ablation abolishes T cell response in vivo [39]. Of note, lamin A/C has potent anti-aging effects (and actually is mutated in the most severe human progeria, Hutchinson-Gilford syndrome) [57], perhaps molecularly connecting to the pro-aging effects of ACBP/DBI. Indeed, aging is (one of) the most important risk factor(s) for cancer diagnosis and progression [58]. Based on the results shown here, it appears possible that the age-related increase in ACBP/DBI might provide one of the molecular links explaining the association between aging and cancer.

Conclusions

Elevations in ACBP/DBI have previously been associated with cardiometabolic risk factors as well as an augmented probability of developing cardiovascular disease [9]. Here, we extend this health-undermining effects of ACBP/DBI to cancer. Clinical associations and experimental interventions suggest that ACBP/DBI favors tumor development/progression through the subversion of immunosurveillance. Indeed, ACBP/DBI neutralization improved the outcome of immunotherapy or chemoimmunotherapy against breast cancer, non-small-cell lung cancer and sarcoma, suggesting but not proving that these findings might apply to other cancers as well. Future investigation must clarify whether ACBP/DBI constitutes a valid target for the prevention or clinical management of neoplastic disease.

Abbreviations

ACBP	Acyl coenzyme A binding protein
AUC	Area under the curve
BMI	Body mass index
CD11c	Integrin alpha X
CD19	B-lymphocyte antigen CD19
CD3	Cluster of differentiation 3
CD4	Cluster of differentiation 4
CD45	Protein tyrosine phosphatase receptor type C
CD8	Cluster of differentiation 8
CT	Chemotherapy
CTL	Cytotoxic t lymphocyte
DBI	Diazepam-binding inhibitor
DEG	Differentially expressed genes
DMBA	Dimethylbenzanthracene
ELISA	Enzyme-linked immunosorbent assay
F4/80	Adhesion G protein-coupled receptor E1
FC	Fold-change
FoxP3	Forkhead box P3
GABA	Gamma-aminobutyric acid
GITR	Glucocorticoid-induced tumour necrosis factor receptor family-related protein
HRP	Horseradish peroxidase
ICOS	Inducible T cell costimulatory
IgG	Immunoglobuline G
KLH	Keyhole limpet hemocyanin
LAG3	Lymphocyte-activation protein 3
Luc	Luciferase
Ly6C	Lymphocyte antigen 6 family member C
Ly6G	Lymphocyte antigen 6 family member G
MPA	Medroxyprogesterone acetate
NK1.1	Killer cell lectin-like receptor subfamily B member 1 C
NSCLC	Non-small cell lung cancer
OVA	Ovalbumin
PD-1	Programmed cell death protein 1
ROC	Receiver operating characteristic
ROI	Region of interest
T_H	Helper T lymphocyte
TIGIT	T cell immunoreceptor with Ig and ITIM domains
Treg	Regulatory T lymphocyte
VISTA	V-set Immunoregulatory receptor

Supplementary Information

The online version contains supplementary material available at https://doi.org/10.1186/s12943-024-02098-5.

Supplementary Material 1

Supplementary Material 2

Supplementary Material 3

Supplementary Material 4

Supplementary Material 5

Supplementary Material 6

Acknowledgements

HC, SZ and MM are supported by the China Scholarship Council. UN-R is supported by Axudas de apoio á etapa de formación posdoutoral da Xunta de Galicia – GAIN. N°Expediente: IN606B-2021/015. TBA received funding from the Odyssea association. The work of IHM and ND is supported by grants from the State Research Agency (AEI, 10.13039/501100011033) of the Spanish Ministry of Science and Innovation (PID2021-122695OB-I00), cofunded by the European Regional Development Fund (ERDF). I.H.-M. is recipent of an FPU fellowship from the Ministry of Science, Innovation and Universities (FPU17/04473). SM is supported by the Erasmus+ mobility funding. GK is supported by the Ligue contre le Cancer (équipe labellisée); Agence National de la Recherche (ANR) – Projets blancs; Association pour la recherche sur le cancer (ARC); Cancéropôle Ile-de-France; Fondation pour la

Recherche Médicale (FRM); a donation by Elior; European Joint Programme on Rare Diseases (EJPRD) Wilsonmed; European Research Council Advanced Investigator Award (ERC-2021-ADG, Grant No. 101052444; project acronym: ICD-Cancer, project title: Immunogenic cell death (ICD) in the cancer-immune dialogue), The ERA4 Health Cardinoff Grant Ener-LIGHT, European Union Horizon 2020 research and innovation programmes Oncobiome (grant agreement number: 825410, Project Acronym: ONCOBIOME, Project title: Gut OncoMicrobiome Signatures [GOMS] associated with cancer incidence, prognosis and prediction of treatment response, Prevalung (grant agreement number 101095604, Project Acronym: PREVALUNG EU, project title: Biomarkers affecting the transition from cardiovascular disease to lung cancer: towards stratified interception), Neutrocure (grant agreement number 861878 : Project Acronym: Neutrocure ; project title: Development of "smart" amplifiers of reactive oxygen species specific to aberrant polymorphonuclear neutrophils for treatment of inflammatory and autoimmune diseases, cancer and myeloablation); National support managed by the Agence Nationale de la Recherche under the France 2030 programme (reference number 21-ESRE-0028, ESR/Equipex+ Onco-Pheno-Screen); Hevolution Network on Senescence in Aging; Institut National du Cancer (INCa); Institut Universitaire de France; LabEx Immuno-Oncology ANR-18-IDEX-0001; a Cancer Research ASPIRE Award from the Mark Foundation; PAIR-Obésité INCa_1873, the RHUs Immunolife and LUCA-pi (both dedicated to France Relance 2030); Seerave Foundation; SIRIC Cancer Research and Personalized Medicine (CARPEM). This study contributes to the IdEx Université de Paris Cité ANR-18-IDEX-0001. The LIFSCREEN study was funded by the French « Ligue contre le Cancer » (grant PRC2010 11588) and sponsored by Gustave Roussy Cancer Campus. We thank the investigators from the LIFSCREEN project for their contribution in data collection, including L. Brugières, S. Foulon, K. Malekzadeh, P. Benusiglio et E. Karamouza. P. Benusiglio has received support from the Swiss National Foundation, grant n°139844. The BRCA1/2 screening study was made possible by the Gynomir grant (INCA-DHOS n°2017-031). High-throughput sequencing was performed by the ICGex NGS platform of the Institut Curie supported by the grants ANR-10-EQPX-03 (Equipex) and ANR-10-INBS-09-08 (France Génomique Consortium) from the Agence Nationale de la Recherche ("Investissements d'Avenir" program), by the ITMO-Cancer Aviesan (Plan Cancer III) and by the SiRIC-Curie program (SiRIC Grant INCa-DGOS-465 and INCa-DGOSInserm_12554). The authors thank the platforms from the Cordeliers Research Center (CFE, CHICS and CGB) and Gustave Roussy Institute (PETRA, PFEP and PFIC) for their help in the histological, cytometric, and animal experimentation techniques throughout the entire project. They thank all participants from the SU.VI.MAX cohort, as well as Pr. Serge Hercberg and Dr. Pilar Galan for their key involvement in the cohort coordination. Recombinant ACBP/DBI was generated by the Biochemistry and Biophysics (B&B) core facility of the Institute of Psychiatry and Neuroscience of Paris (IPNP). We thank Virginie Reynal, Benoit Albaud, Laura Baudrin, and Patricia Legoix at the Curiecoretech Next Generation Sequencing (ICGEX) platform at Institut Curie for the single cell experiments. Data management, quality control and primary analysis of the single-cell RNA sequencing were performed by the Bioinformatics platform of the Institut Curie. Figures were created using BioRender.com.

Author contributions

LM performed most of the experiments, conducted statistical analyses and prepared the figures. PL and LZ performed experiments on TC1 lung cancers. MPL, MM, SZ, SM, JLN, FL, UN-R, HP and JGP contributed to animal experiments. IHM and ND took care of the Trp53 transgenic mice experiments. HC optimized and performed ACBP/DBI-specific ELISAs. LD, MF, MM, BR and LZ provided clinical data. RMO, SB and EP contributed to the design (EP, RMO) and execution (RMO, SB) of scRNAseq experiments. AJ participated to the statistical analyses of patient cohorts. TBA, PB, OC, DB, MD-T, NA, MT and SD provided patient plasma samples and patient information. IM was involved in experimental design and data management. LM and GK wrote the paper.

Funding

HC, SZ and MM are supported by the China Scholarship Council. UN-R is supported by Axudas de apoio á etapa de formación posdoutoral da Xunta de Galicia – GAIN. N°Expediente: IN606B-2021/015. TBA received funding from the Odyssea association. The work of IHM and ND is supported by grants from the State Research Agency (AEI, https://doi.org/10.13039/501100011033) of the Spanish Ministry of Science and Innovation (PID2021-122695OB-I00), cofunded by the European Regional Development Fund (ERDF). I.H.-M. is recipent of an FPU fellowship from the Ministry of Science, Innovation and Universities (FPU17/04473). SM is supported by the Erasmus + mobility funding. GK is supported by the Ligue contre le Cancer (équipe labellisée); Agence National de la Recherche (ANR) – Projets blancs; Association pour la recherche sur le cancer (ARC); Cancéropôle Ile-de-France; Fondation pour la Recherche Médicale (FRM); a donation by Elior; European Joint Programme on Rare Diseases (EJPRD) Wilsonmed; European Research Council Advanced Investigator Award (ERC-2021-ADG, Grant No. 101052444; project acronym: ICD-Cancer, project title: Immunogenic cell death (ICD) in the cancer-immune dialogue), The ERA4 Health Cardinoff Grant Ener-LIGHT, European Union Horizon 2020 research and innovation programmes Oncobiome (grant agreement number: 825410, Project Acronym: ONCOBIOME, Project title: Gut OncoMicrobiome Signatures [GOMS] associated with cancer incidence, prognosis and prediction of treatment response, Prevalung (grant agreement number 101095604, Project Acronym: PREVALUNG EU, project title: Biomarkers affecting the transition from cardiovascular disease to lung cancer: towards stratified interception), Neutrocure (grant agreement number 861878 : Project Acronym: Neutrocure ; project title: Development of "smart" amplifiers of reactive oxygen species specific to aberrant polymorphonuclear neutrophils for treatment of inflammatory and autoimmune diseases, cancer and myeloablation); National support managed by the Agence Nationale de la Recherche under the France 2030 programme (reference number 21-ESRE-0028, ESR/Equipex + Onco-Pheno-Screen); Hevolution Network on Senescence in Aging; Institut National du Cancer (INCa); Institut Universitaire de France; LabEx Immuno-Oncology ANR-18-IDEX-0001; a Cancer Research ASPIRE Award from the Mark Foundation; PAIR-Obésité INCa_1873, the RHUs Immunolife and LUCA-pi (both dedicated to France Relance 2030); Seerave Foundation; SIRIC Cancer Research and Personalized Medicine (CARPEM). This study contributes to the IdEx Université de Paris Cité ANR-18-IDEX-0001. The LIFSCREEN study was funded by the French « Ligue contre le Cancer » (grant PRC2010 11588) and sponsored by Gustave Roussy Cancer Campus. We thank the investigators from the LIFSCREEN project for their contribution in data collection, including L. Brugières, S. Foulon, K. Malekzadeh, P. Benusiglio et E. Karamouza. P. Benusiglio has received support from the Swiss National Foundation, grant n°139844. The BRCA1/2 screening study was made possible by the Gynomir grant (INCA-DHOS n°2017-031). High-throughput sequencing was performed by the ICGex NGS platform of the Institut Curie supported by the grants ANR-10-EQPX-03 (Equipex) and ANR-10-INBS-09-08 (France Génomique Consortium) from the Agence Nationale de la Recherche ("Investissements d'Avenir" program), by the ITMO-Cancer Aviesan (Plan Cancer III) and by the SiRIC-Curie program (SiRIC Grant INCa-DGOS-465 and INCa-DGOSInserm_12554).

Data availability

Patient data were not made publicly available for privacy reasons. Sequences from the single-cell RNA sequencing experiment are available as raw and processed data on GEO (GSE242119). Any additional information required to further analyze data reported in this article will be made available upon request. The pCDH_ZsGreen-OVA_Puro Lenti plasmid generated in this study will made available for non-commercial research purposes upon reasonable request.

Declarations

Ethical approval

The clinical trials (NCT00272428 and NCT01464086) were registered and approved by regular authorities as indicated in the Materials and Methods. Animal experimentation was approved by the local ethics committee at Cordeliers Research Center (project numbers #24410, #31018).

Competing interests

GK have been holding research contracts with Daiichi Sankyo, Eleor, Kaleido, Lytix Pharma, PharmaMar, Osasuna Therapeutics, Samsara Therapeutics, Sanofi, Tollys, and Vascage. GK is on the Board of Directors of the Bristol Myers Squibb Foundation France. GK is a scientific co-founder of everImmune, Osasuna Therapeutics, Samsara Therapeutics and Therafast Bio. GK is in the scientific advisory boards of Hevolution, Institut Servier, Longevity Vision Funds and Rejuveron Life Sciences. GK is the inventor of patents covering therapeutic targeting of aging, cancer, cystic fibrosis and metabolic disorders. One of these patents (co-invented by LM and IM) deals with the use of ACBP/DBI neutralisation for the treatment of cancer. GK's brother, Romano Kroemer, was an employee of Sanofi and now consults for Boehringer-Ingelheim. IM

is a consultant for Osasuna Therapeutics. LZ has held research contracts with Glaxo Smyth Kline, Incyte, Lytix, Kaleido, Innovate Pharma, Daiichi Sankyo, Pilege, Merus, Transgene, 9 m, Tusk and Roche, was on the on the Board of Directors of Transgene, is a cofounder of everImmune, and holds patents covering the treatment of cancer and the therapeutic manipulation of the microbiota. The funders had no role in the design of the study; in the writing of the manuscript, or in the decision to publish the results. The other authors declare no conflicts of interest.

Author details
[1]Centre de Recherche des Cordeliers, Université Paris Cité, Sorbonne Université, Equipe labellisée par la Ligue contre le cancer, Inserm U1138, Paris, France
[2]Metabolomics and Cell Biology Platforms, Gustave Roussy Institut, Villejuif, France
[3]Faculté de Médecine, Université de Paris Saclay, Kremlin Bicêtre, Paris, France
[4]Department of Respiratory and Critical Care Medicine, Union Hospital, Tongji Medical College, Huazhong University of Science and Technology, Wuhan, Hubei, China
[5]Equipe Labellisée Par la Ligue Contre le Cancer, Inserm U1015, Gustave Roussy, Villejuif, France
[6]Department of Pharmacological sciences, University of Piemonte Orientale, Novara, Italia
[7]Grupo de Investigación en Reumatología (GIR), Instituto de Investigación Biomédica de A Coruña (INIBIC), Fundación Profesor Novoa Santos, A Coruña, Spain
[8]Department of Translational Research, Institute Curie Research Center, INSERM U932, PSL Research University, Paris, France
[9]Growth Factors, Nutrients and Cancer Group, Molecular Oncology Programme, Centro Nacional de Investigaciones Oncológicas, CNIO, Madrid 28029, Spain
[10]Institut Curie Genomics of Excellence (ICGex) Platform, Institut Curie Research Center, PSL Research University, Paris, France
[11]Service de Réanimation Médicale, Hôpital Saint-Louis, Assistance Publique Hôpitaux de Paris, Paris, France
[12]Axe cancer, Centre de recherche du Centre Hospitalier de l'Université de Montréal (CRCHUM), Montréal, Canada
[13]Hemato-oncology Division, Centre Hospitalier de l'Université de Montréal (CHUM), Montréal, Canada
[14]Pharmacology Department, Gustave Roussy, Villejuif, France
[15]Department of Cancer Medicine, Gustave Roussy, Villejuif, France
[16]Department of cancer Medicine, « INTERCEPTION » Program for Cancer Prevention, Institut Gustave-Roussy, Villejuif, France
[17]CNRS UMR 9018-METSY, Gustave Roussy and Université Paris-Saclay, Villejuif, France
[18]Department of Thoracic Surgery, Lung Transplantation and Esophageal Diseases, Hôpital Nord, Marseille, France
[19]Faculté des sciences médicales et paramédicales, Aix-Marseille Université, Marseille, France
[20]COMPutational Oncology and pharmacology, Centre de Recherche en Cancérologie de Marseille (CRCM), INRIA-INSERM, Marseille, France
[21]INRAE, CNAM, Nutritional Epidemiology Research Team (EREN), Université Sorbonne Paris Nord and Université Paris Cité, Centre of Research in Epidemiology and StatisticS (CRESS), Inserm, Bobigny F-93017, France
[22]Nutrition, Physical Activity And Cancer Research Network (NACRe Network), Jouy-en-Josas, France
[23]Department of Biology, Center of Clinical Investigations in Biotherapies of Cancer (CICBT), BIOTHERIS, Villejuif, France
[24]Institut du Cancer Paris CARPEM, Department of Biology, Hôpital Européen Georges Pompidou, AP-HP, Paris, France

Received: 27 May 2024 / Accepted: 21 August 2024
Published online: 06 September 2024

References

1. Alquier T, Christian-Hinman CA, Alfonso J, Færgeman NJ. From benzodiazepines to fatty acids and beyond: revisiting the role of ACBP/DBI. Trends Endocrinol Metab. 2021;32(11):890–903.
2. Costa E, Guidotti A. Diazepam binding inhibitor (DBI): a peptide with multiple biological actions. Life Sci. 1991;49(5):325–44.
3. Montégut L, Abdellatif M, Motiño O, Madeo F, Martins I, Quesada V et al. Acyl coenzyme A binding protein (ACBP): an aging- and disease-relevant autophagy checkpoint. Aging Cell. 2023.
4. Marquardt H, Todaro GJ, Shoyab M. Complete amino acid sequences of bovine and human endozepines. Homology with rat diazepam binding inhibitor. J Biol Chem. 1986;261(21):9727–31.
5. Tonon MC, Vaudry H, Chuquet J, Guillebaud F, Fan J, Masmoudi-Kouki O, et al. Endozepines and their receptors: structure, functions and pathophysiological significance. Pharmacol Ther. 2020;208:107386.
6. Bravo-San Pedro JM, Sica V, Martins I, Pol J, Loos F, Maiuri MC, et al. Acyl-CoA-Binding protein is a lipogenic factor that Triggers Food Intake and obesity. Cell Metab. 2019;30(4):754–e679.
7. Joseph A, Moriceau S, Sica V, Anagnostopoulos G, Pol J, Martins I, et al. Metabolic and psychiatric effects of acyl coenzyme A binding protein (ACBP)/diazepam binding inhibitor (DBI). Cell Death Dis. 2020;11(7):502.
8. Joseph A, Chen H, Anagnostopoulos G, Montégut L, Lafarge A, Motiño O, et al. Effects of acyl-coenzyme A binding protein (ACBP)/diazepam-binding inhibitor (DBI) on body mass index. Cell Death Dis. 2021;12(6):599.
9. Montégut L, Joseph A, Chen H, Abdellatif M, Ruckenstuhl C, Motiño O, et al. High plasma concentrations of acyl-coenzyme A binding protein (ACBP) predispose to cardiovascular disease: evidence for a phylogenetically conserved proaging function of ACBP. Aging Cell. 2023;22(1):e13751.
10. Li M, Cao S-M, Dimou N, Wu L, Li J-B, Yang J. Association of metabolic syndrome with risk of Lung Cancer: a Population-based prospective cohort study. Chest. 2024;165(1):213–23.
11. Booth LN, Shi C, Tantilert C, Yeo RW, Miklas JW, Hebestreit K, et al. Males induce premature demise of the opposite sex by multifaceted strategies. Nat Aging. 2022;2(9):809–23.
12. Fabrizio P, Hoon S, Shamalnasab M, Galbani A, Wei M, Giaever G, et al. Genome-wide screen in Saccharomyces cerevisiae identifies vacuolar protein sorting, autophagy, biosynthetic, and tRNA methylation genes involved in life span regulation. PLoS Genet. 2010;6(7):e1001024.
13. Shamalnasab M, Dhaoui M, Thondamal M, Harvald EB, Faergeman NJ, Aguilaniu H, et al. HIF-1-dependent regulation of lifespan in Caenorhabditis elegans by the acyl-CoA-binding protein MAA-1. Aging. 2017;9(7):1745–69.
14. Lamtahri R, Hazime M, Gowing EK, Nagaraja RY, Maucotel J, Alasoadura M, et al. The gliopeptide ODN, a Ligand for the Benzodiazepine site of GABA(A) receptors, boosts functional recovery after Stroke. J Neurosci. 2021;41(33):7148–59.
15. Motiño O, Lambertucci F, Anagnostopoulos G, Li S, Nah J, Castoldi F et al. ACBP/DBI protein neutralization confers autophagy-dependent organ protection through inhibition of cell loss, inflammation, and fibrosis. Proceedings of the National Academy of Sciences. 2022;119(41).
16. Harris FT, Rahman SMJ, Hassanein M, Qian J, Hoeksema MD, Chen H, et al. Acyl-coenzyme A-Binding protein regulates Beta-oxidation required for growth and survival of Non-small Cell Lung Cancer. Cancer Prev Res. 2014;7(7):748–57.
17. Duman C, Di Marco B, Nevedomskaya E, Ulug B, Lesche R, Christian S, et al. Targeting fatty acid oxidation via Acyl-CoA binding protein hinders glioblastoma invasion. Cell Death Dis. 2023;14(4):296.
18. Duman C, Yaqubi K, Hoffmann A, Acikgoz AA, Korshunov A, Bendszus M, et al. Acyl-CoA-Binding protein drives Glioblastoma Tumorigenesis by sustaining fatty acid oxidation. Cell Metab. 2019;30(2):274–89. e5.
19. Caron O, Eleni K, Foulon S, Benusiglio P, Bonadona V, Faivre L, et al. Evaluation of whole body MRI for early detection of cancer in TP53 mutation carriers: final results of the LIFSCREEN study. J Clin Oncol. 2018;36(15suppl):1527.
20. Caron O, Frebourg T, Benusiglio P, Foulon S, Brugières L. Lung adenocarcinoma as part of the Li-Fraumeni Syndrome Spectrum: Preliminary Data of the LIFSCREEN Randomized Clinical Trial. JAMA Oncol. 2017;3(12):1736–7.
21. Hercberg S, Preziosi P, Briançon S, Galan P, Triol I, Malvy D, et al. A primary prevention trial using nutritional doses of antioxidant vitamins and minerals in cardiovascular diseases and cancers in a general population: the SU.VI.MAX study–design, methods, and participant characteristics. SUpplementation en VItamines et Minéraux AntioXydants. Control Clin Trials. 1998;19(4):336–51.
22. Hercberg S, Galan P, Preziosi P, Bertrais S, Mennen L, Malvy D, et al. The SU.VI.MAX Study: a randomized, placebo-controlled trial of the health effects of antioxidant vitamins and minerals. Arch Intern Med. 2004;164(21):2335–42.
23. Robin X, Turck N, Hainard A, Tiberti N, Lisacek F, Sanchez J-C, et al. pROC: an open-source package for R and S + to analyze and compare ROC curves. BMC Bioinformatics. 2011;12(1):77.

24. Montégut L, Chen H, Bravo-San Pedro JM, Motiño O, Martins I, Kroemer G. Immunization of mice with the self-peptide ACBP coupled to keyhole limpet hemocyanin. STAR Protocols. 2022;3(1):101095.
25. Marino S, Vooijs M, van Der Gulden H, Jonkers J, Berns A. Induction of medulloblastomas in p53-null mutant mice by somatic inactivation of rb in the external granular layer cells of the cerebellum. Genes Dev. 2000;14(8):994–1004.
26. Ruzankina Y, Pinzon-Guzman C, Asare A, Ong T, Pontano L, Cotsarelis G, et al. Deletion of the developmentally essential gene ATR in adult mice leads to age-related phenotypes and stem cell loss. Cell Stem Cell. 2007;1(1):113–26.
27. García-Cao I, García-Cao M, Martín-Caballero J, Criado LM, Klatt P, Flores JM, et al. Super p53 mice exhibit enhanced DNA damage response, are tumor resistant and age normally. Embo j. 2002;21(22):6225–35.
28. Buqué A, Bloy N, Perez-Lanzón M, Iribarren K, Humeau J, Pol JG et al. Immunoprophylactic and immunotherapeutic control of hormone receptor-positive breast cancer. Nat Commun. 2020;11(1).
29. Bruchard M, Geindreau M, Perrichet A, Truntzer C, Ballot E, Boidot R, et al. Recruitment and activation of type 3 innate lymphoid cells promote antitumor immune responses. Nat Immunol. 2022;23(2):262–74.
30. Liu P, Zhao L, Senovilla L, Kepp O, Kroemer G. In vivo imaging of Orthotopic Lung Cancer models in mice. Methods Mol Biol. 2021;2279:199–212.
31. Van Eenige R, Verhave PS, Koemans PJ, Tiebosch IACW, Rensen PCN, Kooijman S. RandoMice, a novel, user-friendly randomization tool in animal research. PLoS ONE. 2020;15(8):e0237096.
32. Butler A, Hoffman P, Smibert P, Papalexi E, Satija R. Integrating single-cell transcriptomic data across different conditions, technologies, and species. Nat Biotechnol. 2018;36(5):411–20.
33. Qiu X, Mao Q, Tang Y, Wang L, Chawla R, Pliner HA, et al. Reversed graph embedding resolves complex single-cell trajectories. Nat Methods. 2017;14(10):979–82.
34. Levine AJ. p53: 800 million years of evolution and 40 years of discovery. Nat Rev Cancer. 2020;20(8):471–80.
35. Anagnostopoulos G, Motiño O, Li S, Carbonnier V, Chen H, Sica V, et al. An obesogenic feedforward loop involving PPARγ, acyl-CoA binding protein and GABAA receptor. Cell Death Dis. 2022;13(4):356.
36. Lahalle A, Lacroix M, De Blasio C, Cissé MY, Linares LK, Le Cam L. The p53 pathway and metabolism: the Tree that hides the forest. Cancers (Basel). 2021;13(1).
37. Yang H, Xia L, Chen J, Zhang S, Martin V, Li Q, et al. Stress-glucocorticoid-TSC22D3 axis compromises therapy-induced antitumor immunity. Nat Med. 2019;25(9):1428–41.
38. Liu P, Chen J, Zhao L, Hollebecque A, Kepp O, Zitvogel L, et al. PD-1 blockade synergizes with oxaliplatin-based, but not cisplatin-based, chemotherapy of gastric cancer. Oncoimmunology. 2022;11(1):2093518.
39. Gonzalez-Granado JM, Silvestre-Roig C, Rocha-Perugini V, Trigueros-Motos L, Cibrian D, Morlino G, et al. Nuclear envelope lamin-A couples actin dynamics with immunological synapse architecture and T cell activation. Sci Signal. 2014;7(322):ra37.
40. Saez A, Herrero-Fernandez B, Gomez-Bris R, Somovilla-Crespo B, Rius C, Gonzalez-Granado JM. Lamin A/C and the Immune System: one Intermediate Filament, many faces. Int J Mol Sci. 2020;21(17).
41. Hanahan D. Hallmarks of Cancer: New dimensions. Cancer Discov. 2022;12(1):31–46.
42. Kroemer G, McQuade JL, Merad M, André F, Zitvogel L. Bodywide ecological interventions on cancer. Nat Med. 2023;29(1):59–74.
43. Weeden CE, Hill W, Lim EL, Grönroos E, Swanton C. Impact of risk factors on early cancer evolution. Cell. 2023;186(8):1541–63.
44. López-Otín C, Pietrocola F, Roiz-Valle D, Galluzzi L, Kroemer G. Meta-hallmarks of aging and cancer. Cell Metab. 2023;35(1):12–35.
45. The global burden of cancer attributable to risk factors. 2010-19: a systematic analysis for the Global Burden of Disease Study 2019. Lancet. 2022;400(10352):563 – 91.
46. Correa H. Li-Fraumeni Syndrome. J Pediatr Genet. 2016;5(2):84–8.
47. Mascaux C, Angelova M, Vasaturo A, Beane J, Hijazi K, Anthoine G, et al. Immune evasion before tumour invasion in early lung squamous carcinogenesis. Nature. 2019;571(7766):570–5.
48. Petitprez F, de Reyniès A, Keung EZ, Chen TW, Sun CM, Calderaro J, et al. B cells are associated with survival and immunotherapy response in sarcoma. Nature. 2020;577(7791):556–60.
49. Sharma P, Goswami S, Raychaudhuri D, Siddiqui BA, Singh P, Nagarajan A, et al. Immune checkpoint therapy-current perspectives and future directions. Cell. 2023;186(8):1652–69.
50. Folli F, Guzzi V, Perego L, Coletta DK, Finzi G, Placidi C, et al. Proteomics reveals novel oxidative and glycolytic mechanisms in type 1 diabetic patients' skin which are normalized by kidney-pancreas transplantation. PLoS ONE. 2010;5(3):e9923.
51. Arendt BM, Comelli EM, Ma DW, Lou W, Teterina A, Kim T, et al. Altered hepatic gene expression in nonalcoholic fatty liver disease is associated with lower hepatic n-3 and n-6 polyunsaturated fatty acids. Hepatology. 2015;61(5):1565–78.
52. Styrkarsdottir U, Lund SH, Thorleifsson G, Saevarsdottir S, Gudbjartsson DF, Thorsteinsdottir U, et al. Cartilage acidic protein 1 in plasma associates with prevalent osteoarthritis and predicts future risk as Well as Progression to Joint replacements: results from the UK Biobank Resource. Arthritis Rheumatol. 2023;75(4):544–52.
53. Isnard S, Royston L, Lin J, Fombuena B, Bu S, Kant S et al. Distinct plasma concentrations of Acyl-CoA-Binding protein (ACBP) in HIV progressors and Elite controllers. Viruses. 2022;14(3).
54. Nie X, Qian L, Sun R, Huang B, Dong X, Xiao Q, et al. Multi-organ proteomic landscape of COVID-19 autopsies. Cell. 2021;184(3):775–e9114.
55. Clavier T, Tonon MC, Foutel A, Besnier E, Lefevre-Scelles A, Morin F, et al. Increased plasma levels of endozepines, endogenous ligands of benzodiazepine receptors, during systemic inflammation: a prospective observational study. Crit Care. 2014;18(6):633.
56. Ridker PM, MacFadyen JG, Thuren T, Everett BM, Libby P, Glynn RJ. Effect of interleukin-1β inhibition with canakinumab on incident lung cancer in patients with atherosclerosis: exploratory results from a randomised, double-blind, placebo-controlled trial. Lancet. 2017;390(10105):1833–42.
57. Kubben N, Misteli T. Shared molecular and cellular mechanisms of premature ageing and ageing-associated diseases. Nat Rev Mol Cell Biol. 2017;18(10):595–609.
58. Montégut L, López-Otín C, Kroemer G. Aging and cancer. Mol Cancer. 2024;23(1):106.

Publisher's note